NASA CR- 152480

The
Bendix
Corporation

Research
Laboratories

Southfield, Michigan
48076

BRL Project 4564

Final Technical Report
MSS Image Data Study

September 30, 1976

Prepared Under:
Contract No.
NAS-22366

Submitted to:

National Aeronautics &
Space Administration
Goddard Space Flight Center
Greenbelt, Maryland 20771

Prepared by:

W. F. Derouchie
Project Supervisor

Approved by:

W. E. Chapelle
Director
Photogrammetry Program

Report No. 8272
Copy No. 5

Bendix Research Laboratories

The
Bendix
Corporation

Research
Laboratories

Southfield, Michigan
48076

BRL Project 4564

Final Technical Report
MSS Image Data Study

September 30, 1976

Prepared Under:
Contract No.
NAS-22366
5.

Submitted to:

National Aeronautics &
Space Administration
Goddard Space Flight Center
Greenbelt, Maryland 20771

Prepared by:

W. F. Derouchie
Project Supervisor

Approved by:

W. E. Chapelle
Director
Photogrammetry Program

Report No. 8272
Copy No. 5

1 INTRODUCTION AND SUMMARY

The overall objectives of this study were (1) to define the attitude behavior of the LANDSAT 1 satellite, together with attitude-like effects imparted by the MSS internal geometry; and (2) from this information, to develop the necessary control point spacing for achieving different desired accuracies for a single MSS pass over an area the size of the continental U.S.

The analysis was performed for a continuous swath of 11 LANDSAT 1 MSS images, representing about 5 minutes of elapsed time and 2000 km in distance. Control points, selected from published large-scale topograph maps, were compared with the image data to determine the image positioning errors. The results of the analysis were checked by analysis of a second image pass covering the same area.

A comprehensive mathematical model which includes orbital constraints and high frequency attitude effects was developed, to relate ground and image locations. The parameters of this model were derived from known ground locations of image identifiable points. It should be stressed that the term attitude effect, as used here, includes attitude like effects. For example, high frequency positional effects due to gravity anomolies are indistinguishable from attitude effects.

The accuracy achieved, using a very dense pattern of control points, is approximately 60 meters RMS, for both passes. This is true even though the low frequency attitude errors have very different amplitudes. A minimum control point spacing of 100-150 MSS mirror sweeps (50 to 70 km) was necessary to achieve circular accuracies on the order of 100 meters RMS. More points than this would be necessary if control point identification and measurement errors were to be detected.

2 IMAGERY USED

A LANDSAT pass containing 11 scenes from Traverse Bay, Michigan to New Orleans, Louisiana was selected. This area has two mostly cloud-free coverages, one in May of 1973 and the other in October of 1974. The scenes used have identification numbers of 1285-15583 to 1285-16024, and 1825-15463 to 1825-15504.

This area was chosen for its nearly complete coverage by 1/24,000 maps, and the abundance of small lakes, rivers, and other well defined land-water interfaces. This type of feature makes an excellent ground control point, since it is quite permanent, easy to identify, and tends to be symmetric. Symmetry is quite important. The human visual system has great ability to repeatedly locate the center of an object.

Band 7 (MSS band 4) was chosen for exclusive use in this study. This imagery offers the best definition of land water interfaces. To keep the number of sensor related parameters to a minimum, it was not desirable to use more than one spectral band.

3 CONTROL POINT SELECTION

The objective was to select control point data for the modeling of the MSS imaging process, and the measurement of associated errors. Three steps were used in gathering control point data. First, control points were selected from source maps corresponding to LANDSAT film images. Then, control point earth coordinates were determined by digitizing the source maps on the Bendix System 100, which uses a Datagrid digitizer. Finally, the control points were located in the LANDSAT digital image by pointing in this image as displayed on a CRT monitor, part of the Bendix Experimental Photogrammetric Facility. These three steps represent coordinate transformations from (X,Y) source map position, to earth-based geometric coordinates, and finally to line a pixel position in the LANDSAT digital image.

USGS source maps provided almost complete coverage of the outer quarter of the imagery on each side of the image strip. These maps were primarily at 1/24,000 scale. About 10 percent of the maps were at 1/62,500 scale.

From the source maps, 630 control points were selected. These points were distributed fairly evenly throughout both outer quarters of the image strip. Image edge information is best for indicating spacecraft yaw variations, while pitch and roll effects are positionally invariant in the image.

The control points selected are mostly of the following general types:

a. Small bodies of water
b. Reasonably symmetric points of land or bays of water
c. River or canal intersections
d. Inlets or outlets of lakes
e. Islands

Each control point has been circled on a map (see Figure 1 for an example) and on an enlarged paper print of the LANDSAT imagery. In addition a sketch of each point was made at the time of selection to further assist in the subsequent measurement procedure. The sketches include a precise definition, by a dot, of the exact point to be measured. The sketch is accompanied by a verbal definition e.g., Shake Point, Round Lake, etc.

4 CONTRO: POINT MEASUREMENT

The ground coordinates were obtained for each control point using the Bendix System 100. The associated Datagrid® digitizer, accurate to 0.002 inch, is used to digitize the points, and the latitude and longitude of each point is automatically interpolated. This interpolation has the form:

$$X = a_0 + a_1 X + a_2 Y + a_3 XY$$

$$Y = b_0 + b_1 X + b_2 Y + b_3 XY$$

Each USGS map has 16 reference marks equally spaced in geographic coordinates. For a 1/24,000 scale map, the interval in latitude and longitude is 2-1/2 minutes. The interval is 5 minutes for a 1/62,500 scale map. For every control point or points on a source map, the four closest surrounding reference marks are digitized. From these marks, the geodetic coordinates of the control point are interpolated.

The actual point to be measured was determined by visual inspection with the aid of the sketch prepared when the point was initially selected. Approximately 80% of the control points selected were found on individual source maps. It is estimated that the total circular standard error for the maps and digitization process is less than 8 meters for control points from the 1/24,000 maps, and less than 18 meters for those from 1/62,500 maps.

Each LANDSAT image is represented by four digital tapes dividing the scene into four vertical swaths. The overlap between scenes is about 7 percent. Digitally, LANDSAT images are 3240 pixels in the column direction (cross-track or east-west) and 2340 pixels in the row direction (along-track). A pixel in a LANDSAT image represents an earth area of approximately 60 by 80 meters.

To find a control point on a digital image tape, it proved desirable to display the digital image on a CRT display. The Bendix Experimental Photogrammetric Facility was used to determine the approximate line and pixel location of a control point and then display the surrounding image on the facility's CRT monitor.

The 70 millimeter MSS image was placed on one XY measuring stage. The line and pixel coordinates of the 4 image corners are known, and the X, Y stage location measured. From this a simple transformation from stage XY to line and pixel is determined. Subsequently, as each control point is visited, the computer translates the XY location into an approximate line and pixel location.

Next, one of four digital magnetic tapes corresponding to the MSS image was used to display the image area for each control point on the CRT monitor. Alphanumeric characters used to represent image grey levels were (-1ZS8M*) in addition to the "blank" character. Rarely do all the 64 grey levels appear for the image area around a control point, so the 8 characters were dynamically assigned to grey level ranges. That is, if only the grey levels 2 through 33 appeared, then the "blank" is assigned to levels 2-5, the "-" is assigned to levels 6-9, etc.

The display area on the CRT monitor consists of 23 rows and 37 columns. In addition, three levels of image display are used: a reduced display for initial location, a normal size display, and an enlarged display for final pointing. For the enlarged display, the data is resampled by means of a bilinear interpolation. This does not improve the resolution of the display, but does allow for quantifying the line and pixel units to fractional parts of their original size. Figures 2 through 4 show the three display scales for an area around the control point in Figure 1.

For each display size, a pointer in the display may be moved around to locate the position of a control point. Successively, the area around the pointer is increased to normal image size and then enlarged. The pointer is repositioned as necessary and the pixel and line location recorded. With measurements made in units of one-third of a line and one-half of a pixel,the equivalent ground resolution of the final enlarged display is about 30 meters. Thus the recorded image locations are to the nearest 15 meters. The exact control point location was determined by visual inspection, with the aid of the sketch made when the point was originally selected.

Since some control points exist in overlap areas between MSS images, some control points were measured on more than one digital tape. In this manner, the amount of overlap between MSS images was determined and the appropriate translations made to create a continuous strip coordinate system.

A total of 435 control points were measured in the first pass imagery, and 331 in the second pass. The remaining points could not be measured due to poor image definition. On the second pass many points did not appear due to offset between the passes.

5 MATHEMATICAL MODEL

The orientation model was divided into two distinct segments. First, a basic model was used to relate ground position with image location. The basic model included sensor location, internal sensor parameters, and parameters for low frequency attitude angle effects with a frequency less than one cycle over the 11-scene strip.

The residual control point errors, remaining after determination of the basic model parameters, were analyzed for higher frequency attitude (pitch, roll, yaw) effects in the attitude angle model.

5.1 Basic Model

The orientation elements established for the basic model were of two general types, those related to the spacecraft/sensor platform and those related to the sensor.

The orientation elements related to the spacecraft are time-dependent and were treated as a function of the mirror sweep number within the image strip. Assumptions explicit here are that the mirror sweep cycle time does not vary and that the spacecraft orientation does not vary (significantly) during a single sweep. Thus, the six scan lines imaged during a single mirror sweep share the same spacecraft orientation.

Following are the orientation elements of the spacecraft/sensor:

- Geodetic latitude
- Geodetic longitude

- Spacecraft height above the earth ellipsoid, measured along the local vertical
- Yaw angle with respect to instantaneous orbit heading
- Roll angle with respect to local vertical
- Pitch angle with respect to local vertical

The sensor-related orientation parameters were confined to across-track look angle as a function of pixel number (mirror velocity) , and detector spacing.

To aid in the separation of locational and attitude effects, the latitude and longitude (Φ, L) of the spacecraft were confined to lie in an orbital plane. The orbital model used is relatively simple, due to: (1) the short orbital arc that must be modeled, and (2) the fact that pitch and roll errors are virtually indistinguishable from along- and across-track errors, insofar as they affect the imagery.

To find (Φ, L), the orbital angle (ε), see Figure 5, must first be determined. This angle is measured at the earth's center, from the terminator to the current satellite position. The angle θ was computed as follows:

(1) $$\theta = \omega_o t + C_5$$

where ω_o = angular velocity

t = time from reference point

C_5 = an unknown orbital angle from the terminator to the reference point

The angular velocity (ω_o) is found from

(2) $$\omega_o = C_1 + C_2 t$$

where C_1 and C_2 are carried as unknowns to be determined. Angular velocity ω_o was allowed to vary as a function of time to compensate for the known ellipsoidal shape of the earth and orbit.

The time (t) is the time from the reference point and is determined directly from the MSS mirror sweep number (S) as

(3) $$t = S/13.62$$

The reference point is selected to be the center of an MSS mirror sweep which is approximately at the center of the image strip. The sweep number (S) is the difference in lines between the control point and the reference point, modulo 6.

Once θ has been determined, longitude L can be computed from

(4) $$L = \tan^{-1}\left[\frac{\tan\theta}{\sin(C_3)}\right] + C_4 + R_e t$$

where

C_3 = the unknown orbital inclination (measured at the poles) which must be determined

C_4 = the unknown longitude of the terminator, which must be found

R_e = rotational rate of the earth (degrees per unit time

The spacecraft altitude (H), the distance along the local vertical from the earth ellipsoid to the spacecraft, was carried as the function

(5) $$H = C_{12} + C_{13}\,t + C_{14}\,t^2 + C_{15}t^3$$

where C_{12} through C_{15} are unknown coefficients to be determined. H is allowed to vary to compensate for the ellipsoidal nature of the earth and the actual spacecraft orbit.

The latitude (Φ) can be computed from:

$$\Phi = \tan^{-1}\left[\left(\frac{a^2 + aH}{b^2 + aH}\right)\left(\frac{\cos\theta \cos C_3}{(\sin^2\theta + \cos^2\theta \sin^2 C_3)^{1/2}}\right)\right] \tag{6}$$

where
- a = semi-major axis of earth ellipsoid
- b = semi-minor axis of earth ellipsoid
- H = spacecraft altitude

The orientation parameters related to the sensor were confined to (a) the across-track look angle (ω') which is carried as a function of the pixel number J along an image line, with J = 0 at the line center:

$$\omega = C_6 J + C_7 J^2 + C_8 J^3 \tag{7}$$

and (b) the along-track detector spacing (P_o), which is treated as a function of the detector number (n), within a mirror sweep:

$$P_o = C_{16} n \tag{8}$$

The low frequency yaw (K) effects were modeled as a function of time as

$$K = C_9 + C_{10} t + C_{11} t^2 \tag{9}$$

where C_9 - C_{11} are unknown coefficients to be determined.

The low frequency pitch (ϕ) effects were modeled as a function of time as

$$\phi = C_{17} t^2 \tag{10}$$

The low frequency roll (ω) effects were modeled as a function of time as

$$\omega = C_{18}\, t^2 \tag{11}$$

It is very important to note that no 'zeroth' order, or constant term is contained in (10) or (11). This is entirely due to the narrow angular field of view of the MSS sensor. For small angles, a resolution far greater than that afforded by the MSS is necessary to separate angular from positional displacement. A constant pitch or roll angle simply can not be distinguished from a constant positional offset.

The first order (linear) term is not present in (10) or (11) because they are highly correlated with the orbital velocity and inclination, respectively.

A set of orientation parameter coefficients (C_i) can be determined from points whose image location (line, pixel), and ground coordinates (latitude, longitude, and elevation) are known. This is done by solving the error equations, which can be generated for such known points.

For each control point the applicable orientation parameters can be calculated from the known line and pixel location using equations (1) to (9). The next step in forming the error equations is the establishment of an auxiliary local cartesian coordinate system with origin at the sub-orbital point (Φ , L) and sea level, tangent to the earth ellipsoid. This system is right handed with +Z up and +X axis perpendicular to the sweep direction and nominally south. The actual angle between the +X axis and south is the sum of orbit heading and the yaw angle. The orbit heading angle is derived from the derivatives of Φ and L with respect to time. The sub-orbital point is found by using the known line number of the control point to solve equations (1) thru (6).

The first step in determining the error at a control point is the determination of its coordinates (X_L, Y_L, Z_L) in the local coordinate system described above.

Next, the measured line and pixel is used to compute an estimate of the control points X and Y coordinates (XE, YE) in the local coordinate system. These coordinates are determined, in the plane defined by the known elevation of the control point in the local system (Z_L):

(12)
$$X_E = (\tan(\phi) + P_o)(H - Z_L)$$

$$Y_E = (\tan(\omega + \omega'))(H - Z_L)$$

where H, ω Po, ϕ, and ω are determined from equations (5), (7), (8), (10), and (11).

Errors due to inadequacies in the imaging model appear as

(13)
$$\epsilon_X = X_E - X_L$$

$$\epsilon_Y = Y_E - Y_L$$

Error equations describing the relationship between ϵ_X, ϵ_Y, and the orientation element coefficients (C_i) can be expressed in linear form (for each control point) as:

(14)
$$\frac{\partial X}{\partial C_1}\Delta C_1 + \frac{\partial X}{\partial C_2}\Delta C_2 + \cdots \frac{\partial X}{\partial C_{18}}\Delta C_{18} = \epsilon_X$$

$$\frac{\partial Y}{\partial C_1}\Delta C_1 + \cdots + \frac{\partial Y}{\partial C_{18}}\Delta C_{18} = \epsilon_Y$$

where ϵ_X and ϵ_Y, from equations (13), are along- and across-track errors obtained using the current approximation to the orientation element coefficients C_j, detailed in equations (1) to (11). The ΔC_i are the adjustments for these coefficients which will ideally make ϵ_X and ϵ_Y zero.

The partial derivatives in (14) are difficult to derive explicitly, so they were approximated numerically. The approximation technique used was to perturb each C_i a small amount and evaluate the model to determine the effect on the X and Y error (ϵ_X, ϵ_Y). The ratio of the change in error to the coefficient perturbation was used as the partial derivative.

A pair of equations (14) can be formed for each control point. This large set of equations can be reduced to 18, "normal equations", one for each unknown C_i. The normal equations are then solved for the ΔC_i.

The solution for the final coefficients C_i is an iterative one, involving repeated formations of the normal equations and solution for new coefficient changes, ΔC_i. This solution procedure is terminated when the RMS of the error over all points fails to decrease significantly (0.1 meter).

A recap of the procedure used to determine the orientation element coefficients (C_i) follows. Step I to VIII are performed for each control point.

I Compute the mirror sweep number from line number

II Find line number (modulo 6) within sweep

III Reference pixel number to center of line and determine across track look angle

IV Use mirror sweep number and current orientation element coefficients to determine sensor location Φ, L, H, and attitude

V Compute the actual coordinates of the control point in the LSR system with origin at (Φ, L, H = 0)

VI Estimate the (X, Y) LSR coordinates at the elevation of the control point, from the image location

VII Determine error of the control point -- actual (X, Y) LSR coordinates minus the estimates

VIII Perturb in sequence the orientation element coefficients and form the normal equations

IX Solve the normal equations for corrections to the coefficients

X Repeat the above steps until the RMS of the error determined in VII fails to decrease

5.2 ATTITUDE ANGLE MODEL

The residual ϵ_X and ϵ_Y errors resulting from the final parameters for the basic model were converted to equivalent pitch and roll errors, that is, the amount of pitch and roll which would be required to set ϵ_X and ϵ_Y to zero.

These equivalent pitch and roll angles were modeled as smooth, continuous functions of time. The final errors resulted from applying these smoothed attitude angle functions at each point.

Both the along-track and across-track errors from the basic model exhibited strong sinusoidal appearance when plotted as functions of along-track position. This suggested the use of a truncated Fourier series to model the systematic errors. The equivalent pitch and roll data was transformed to frequency domain representations using a Discrete Fourier Transform. Spatial domain representations were then regenerated using frequency spectrum truncation (low-pass filtering).

To obtain a meaningful Fourier transform of this data, some additional data preparation was required. Since the Discrete Fourier Transform treats the data as being cyclic, discontinuities at the ends of the interval should be removed. This was done by extending the interval slightly and adding a point at each end

which had zero errors. The original data covered a range of approximately $\pm$1900 mirror sweeps. Points were added at $\pm$2000 mirror sweeps to remove discontinuities at the ends and still preserve the exact values of the original error data points.

Since the Discrete Fourier Transform is simply a linear mapping of one set of points into another, the transform of the sorted points could have been taken directly, but it was not because certain physical significance would have been lost. The sorted points are irregularly spaced in time, whereas the transformation should be performed on regularly spaced data. With regularly spaced input data, the frequency spectrum components can be directly related to oscillatory motion of the spacecraft/sensor as a function of time.

To obtain regularly spaced input data, the data points were linearly interpolated to 400 regularly spaced points with a spacing of 10 mirror sweeps. The interpolated point set was then transformed using a Discrete Fourier Transform. The Discrete Fourier Transform maps the input points (f_i) into Fourier coefficients a_k, b_k as follows:

$$(15) \qquad a_k = \frac{1}{N} \sum_{i=0}^{2N-1} (f_i) \cos \frac{k\pi i}{N}, \; k = 0, 1, 2 \ldots N$$

$$b_k = \frac{1}{N} \sum_{i=0}^{2N-1} (f_i) \sin \frac{k\pi i}{N}, \; k = 1, 2 \ldots N-1$$

The 2N input points are mapped into N pairs of frequency domain coefficients. The original input sampled data function can then be represented by the series:

$$(16) \qquad f_i = \frac{a_o}{2} + \sum_{k=1}^{N-1} \left[a_k \cos \frac{k\pi i}{N} + b_k \sin \frac{k\pi i}{N} \right] + \frac{a_N}{2} \cos \pi i$$

This exactly represents the input data to the Fourier transform program, which is the interpolated point set. A slightly modified scheme was used for the error model to obtain a continuous function which could be compared with the original irregularly spaced data. The Fourier coefficients determined from the Discrete Fourier Transform were used to determine a continuous function as follows:

$$(17) \qquad f(x) = \frac{a_o}{2} + \sum_{k=1}^{M} \left[a_k \cos k2\pi \left(\frac{x-x_1}{x_2 - x_1} \right) + b_k \sin k2\pi \left(\frac{x-x_1}{x_2 - x_1} \right) \right]$$

In general, the series was truncated with $M \leq N-1$, and the last coefficient a_N was not used. Truncating this series discards the high frequency components above a certain limit. This effectively produces a low-pass filtering effect. After having generated the frequency spectrum coefficients a_k and b_k, applying various amounts of filtering in the model is very simple since it only involves truncating the above series at different values of M. The frequency spectrum of the errors is, of course, also of interest since it gives additional insight into the nature of the systematic errors.

To determine residual errors between the original error data and the truncated Fourier Series Model, the continuous model function was evaluated at the coordinates of the original irregularly spaced data points. At each point, the value of the smoothed function was subtracted from the original error value to determine the residual. The RMS of these residuals was then calculated.

The final Y (across-track) error εy_f for a point is computed as

(18) $$\varepsilon y_f = \varepsilon_Y - H\omega_{tf}$$

where

ε_Y = Y error from basic model

H = *spacecraft altitude*

ω_{tf} = roll angle computed from the truncated Fourier series representing roll.

The X (along-track) errors εX_{fi} resulting from the application of the truncated pitch Fourier series

(19) $$\varepsilon X_{fi} = \varepsilon_X - H\ \phi_{tf}$$

where

ε_X = X error from basic model

H = spacecraft altitude

ϕ_{tf} = roll angle computed from the truncated Fourier series representing pitch

were further processed to determine high frequency yaw effects. The εX_{fi} values were converted to equivalent yaw values and modeled with a truncated Fourier series. The effects of the small yaw angles on across-track errors is insignificant.

The final along-track errors ϵx_f are computed as

(20) $$\epsilon x_f = \epsilon X_{fi} - Y k_{ft}$$

where

ϵX_{fi} = errors after pitch correction

Y = across-track distance from orbit ground track

k_{ft} = yaw angle from truncated Fourier series representing yaw.

6 ANALYSIS

6.1 FIRST PASS

A total of 356 points were finally used for the analysis of the image errors for the first pass. These points are plotted in Figure 6. The remaining measured image points were discarded due to very large errors caused by misidentification or blunders.

The solution for the parameters of the basic math model produced RMS errors of 484 meters along track and 316 meters across track. The errors, plotted in Figures 7 and 8, show a high amplitude, relatively low frequency distribution.

The discrete Fourier transforms of the equivalent attitude angles, as described in Section 5.2, were then computed. The frequency spectra of the attitude angles are shown in Table 1. Only the first 30 components are shown, as most of the power is contained in the first few terms.

Pitch and roll functions were produced by truncating the Fourier series at 15 terms for pitch and roll, and 8 terms for yaw. The cutoff at 15 terms was chosen

somewhat arbitrarily. All the significant terms are included, and it allows for a component having about a period of somewhat less than one MSS scene. The yaw series was truncated at 8 terms, to be consistent with the 15 terms for pitch and roll. It takes twice as many points, half on each side to determine yaw.

The errors remaining after the application of these truncated Fourier series are plotted in Figures 9 and 10. The RMS along track is 65 meters, and across track is 67 meters.

Figures 11 through 15 are plots of pitch, roll, yaw, spacecraft elevation, and mirror velocity non-linearity. The mirror non-linearity plot shows the discrepancy from a uniform angular velocity.

The relationship between along track spacing and achievable accuracy was studied next. Subsets of points were selected according to a spacing criterion. The basic and detailed math models were then determined. The resulting model was then applied to all the points, to determine an accuracy figure.

The point subsets were selected by a programmed algorithm, thus eliminating any human biases in the selection process. This algorithm attempted to select points on alternating sides of the strip, to maximize the capability to model yaw angles.

Spacings along strips of 50, 100, 150, and 200 mirror sweeps were evaluated. The results of these four subsets, as well as those from all the points, are summarized in Table 2. In addition to giving RMS errors, and reference to point plots Table 2 shows the truncation point for the attitude angle Fourier series and whether or not the mirror velocity and sensor spacing parameters were solved for. For spacings of 150 and 200 mirror sweeps these sensor calibration parameters were not solved for, due to the small number of points. Instead the parameters determined for the 100 sweep subset were used. For the 200 mirror sweep spacing the Fourier series for pitch and roll were truncated at 10 terms, and that for yaw at 5 terms. These truncation points were changed because there was no longer sufficient information to use the higher truncation points.

6.2 SECOND PASS

After completion of the analysis for the first pass, the second pass imagery was analyzed. Identical operations were performed with this data as with the first image pass.

Many points were measured on this imagery which could not be measured on the first pass. However, many more either could not be measured on this pass or were lost due to the slight misalignment of the two imaging passes. A total of 262 points were considered usable on the second image pass. These points are plotted in Figure 20. The RMS errors after determination of the basic model parameters were 155 meters along track and 151 meters across track.

Tables 3 and 4 contains the same information for this analysis as Tables 1 and 2 do for the first pass. Figures 21 and 22 show the errors after finding the parameters for the basic model while Figure 23 and 24 show the final errors after removal of the high frequency attitude effects. Figures 25 through 29 show the modeled pitch, roll, yaw, spacecraft altitude, and mirror velocity nonlinearity for the second pass.

As can be seen from the plot in Figures 21 and 22, the errors attributable to attitude effects are much smaller, with a smoother distribution. The final errors for all points are not proportionately better, indicating the two passes share high frequency limiting errors.

The most significant difference between the first and second passes is the relatively small number of points necessary to achieve a given accuracy level on the second pass.

7 DISCUSSION AND CONCLUSIONS

First, a review of the numbers of control points used is in order before drawing conclusions on the number of control points needed to control a strip of

MSS imagery of this length. Initially 630 control points were identified by visually correlating the film imagery with the maps. Only 435 points could actually be measured in the digital imagery of the first pass. And of the measured ones, only 356 were judged free of measuring errors or blunders. It was this "clean" set of points which were sampled to provide the subsets for the various point spacings. The relationships between point spacing and achievable accuracy stated in this report must be considered ideal. When selecting points initially at least 50% more points than indicated by spacing requirements should be selected for a given accuracy level. This will allow for removal of points which have been incorrectly identified or measured.

The use of a Fourier series to model the attitude systematic error function provides a general relationship between control point spacing and the degree of attitude error compensation. Basically, the nominal control point spacing determines the highest frequency component which can be determined. The period of the highest frequency which can possibly be detected by ground control points is twice the nominal point spacing. This relationship is not affected by amplitude until the amplitude decreases to the point where it approaches the inherent error in the control point itself. The RMS (RMS_{hf}) effect of all higher frequencies is

$$RMS_{hf} = \sqrt{\Sigma (A_i^2/2)}$$

where A_i is the amplitude of these higher frequency components.

The two image passes analyzed for this study provide an excellent example of what happens when the amplitudes of all frequency components are changed. Tables 1 and 3 show that the shape of the frequency attitude spectra for both passes is very similar. However, the power in each frequency component reflects the differences in the RMS error attributable to attitude error components. (The RMS error is the square root of the power tabulated in the table multiplied by the 920,000 meter height.)

The reduction in frequency component amplitude (especially pitch) is evident in the relationship of RMS error (along track) and control point spacing shown in Tables 2 and 4. This higher amplitude of all pitch frequency components makes the correct determination of higher frequency components more important. More control points are necessary for this determination.

The first pass can probably be regarded as anomalous since the attitude, especially pitch, values are significantly higher than expected. For both passes the pitch angle frequency components have greater amplitude than those for roll, thus making the correct determination of the pitch function more important. The relative amplitude of the yaw frequency components is relatively high. This is not critical, because the "lever arm" for yaw is only 50 kilometers (at image edge). Pitch and roll have a "lever arm" of about 920 kilometers. In fact, the determination of yaw components, beyond the basic model, only improves the along-track RMS by 5 to 10 meters.

The RMS errors shown for all points in Table 2 and 4 are a function of at least the following:

a. Map errors
b. Imaging errors
c. Image measurement uncertainties
d. Measurement error
e. Uncompensated attitude effects

Map errors include not only the errors made in map production, but also the fact that maps only represent what was at some point in time. Natural processes act to change the size, shape and even location of natural features. Seasonal changes alone have a significant effect. These errors are the ultimate limiting factor when using maps to determine the location of ground control.

Imaging errors include mechanical sensor imperfections, such as mirror wobble, but also radiometric imperfections. These imperfections are partly related to resolution element size and partly to response time, i.e. when (where) an abrupt transition is actually imaged. Thus, a well defined feature such as a land water interface may not be detected correctly spatially.

Image measurement uncertainties are due to a collection of causes which could be categorized under map or imaging errors. They haven't been because they deal specifically with the interpretation and matching of imagery to map information.

Measurement error includes both the human error in measuring and the resolution limit of 1/2 the least count in the measuring process.

All remaining errors may be attributable to uncompensated attitude effects (or attitude like effects). How large are these errors? Experience and common sense leads to the assignation of 20 meters RMS to each of the other error sources, or a combined RMS of 40 meters. Forty to forty-five meters RMS is therefore attributable to the uncompensated attitude errors. These errors are spread across the higher frequencies of the attitude effect spectrums.

While the study demonstrated that an MSS image strip can be controlled to about 60 meters RMS, the dense net of control points required makes this level of accuracy clearly impractical for an operational system. Accepting 100 meters RMS as a more reasonable goal, a minimum control point spacing of 100-150 mirror sweeps (50 - 70 kilometers) should be adequate.

The above conclusion is consistent with the spectral analysis, which shows the large component amplitudes concentrated below the 10-cycle component. Spatial periods in this range are about 400 mirror sweeps and above. Thus, control point spacings of 200 mirror sweeps or less should be required.

COMPONENT	POWER		
	PITCH $\times 10^{-7}$	YAW $\times 10^{-7}$	ROLL $\times 10^{-8}$
0	.016	3.031	.0007
1	.143	1.200	1.36
2	.379	.778	6.58
3	1.305	1.054	2.89
4	.830	.383	2.51
5	.053	.0060	.021
6	.065	.407	.009
7	.323	.252	.019
8	.060	.496	.003
9	.016	.213	.001
10	.028	.180	.021
11	.033	.246	.036
12	.023	.0041	.019
13	.021	.159	.00004
14	.035	.010	.029
15	.0009	.226	.024
16	.0042	.346	.075
17	.0043	.376	.031
18	.013	.126	.007
19	.0037	.378	.023
20	.016	.161	.003
21	.016	.052	.00003
22	.028	.055	.0001
23	.0023	.063	.001
24	.014	.220	.007
25	.0010	.052	.004
26	.014	.053	.004
27	.0005	.138	.006
28	.0011	.037	.001
30	.0004	.106	.002

Table 1 - Frequency Spectra For First Pass Attitude

	Point Spacing In Mirror Sweeps				
	All Points	50	100	150	200
Sensor Calibration	Yes	Yes	Yes	No	No
Pitch Series Cut-Off (Number of Terms)	15	15	15	15	10
Roll Series Cut-Off (Number of Terms)	15	15	15	15	10
Yaw Series Cut-Off (Number of Terms)	8	8	8	8	5
Plot of Points Used (Figure No.)	6	16	17	18	19
Along Track RMS (meters)	65	104	116	147	158
Across Track RMS (meters)	67	87	89	90	96

Table 2 - Summary of First Pass Analysis Results

	POWER		
COMPONENT	PITCH $\times 10^{-8}$	YAW $\times 10^{-7}$	ROLL $\times 10^{-9}$
0	.0011	.171	.159
1	.041	2.158	1.879
2	.183	.032	3.761
3	.439	.465	8.957
4	1.061	1.185	5.270
5	.024	.322	.306
6	.0012	.155	1.193
7	.073	.343	.360
8	.015	.470	.364
9	.020	.081	.839
10	.062	.0071	.045
11	.0019	.139	.032
12	.024	.335	.045
13	.0001	.079	.033
14	.0040	.046	.0031
15	.012	.024	.0006
16	.0094	.283	.0005
17	.0009	.169	.0074
18	.0057	.032	.022
19	.0045	.033	.0016
20	.018	.012	.00003
21	.0044	.106	.0053
22	.0007	.036	.0009
23	.0002	.014	.0013
24	.0003	.050	.0005
25	.0039	.0049	.0026
26	.0060	.020	.0094
27	.0043	.0071	.0009
28	.0037	.078	.0003
29	.0093	.0097	.013
30	.0068	.072	.0065

Table 3 - Frequency Spectra For Second Pass Attitude

	Point Spacing in Mirror Sweeps				
	All Points	50	100	150	200
Sensor Calibration	Yes	Yes	Yes	Yes	No
Pitch Series Cut-Off (Number of Terms)	15	15	15	15	10
Roll Series Cut-Off (Number of Terms)	15	15	15	15	10
Yaw Series Cut-Off (Number of Terms)	8	8	8	8	5
Plot of Points Used (Figure No.)	20	30	31	32	33
Along Track RMS (meters)	53	77	93	74	158
Across Track RMS (meters)	58	77	78	84	116

Table 4 - Summary of Second Pass Analysis Results

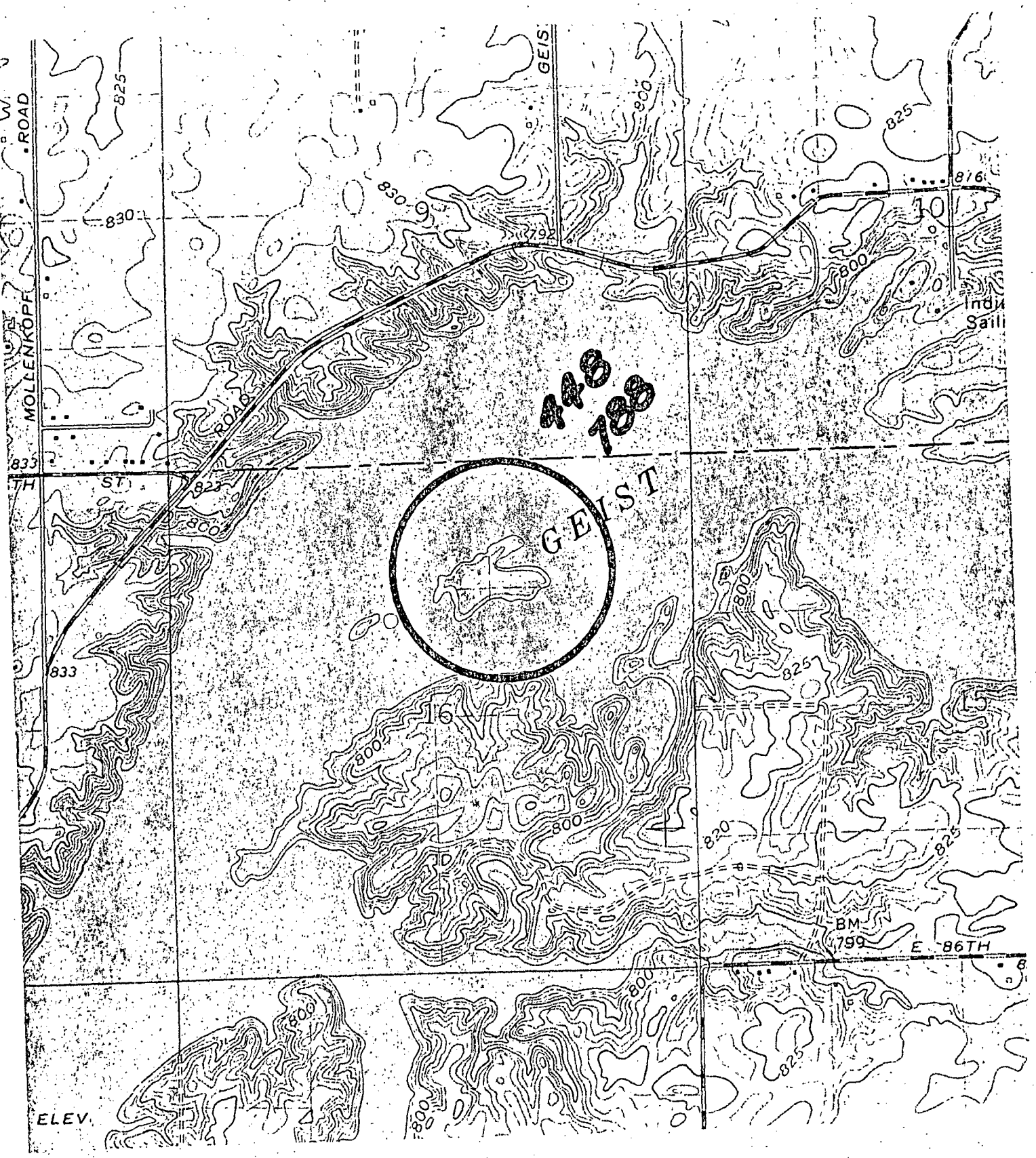

Figure 1 - Typical Map Control Point

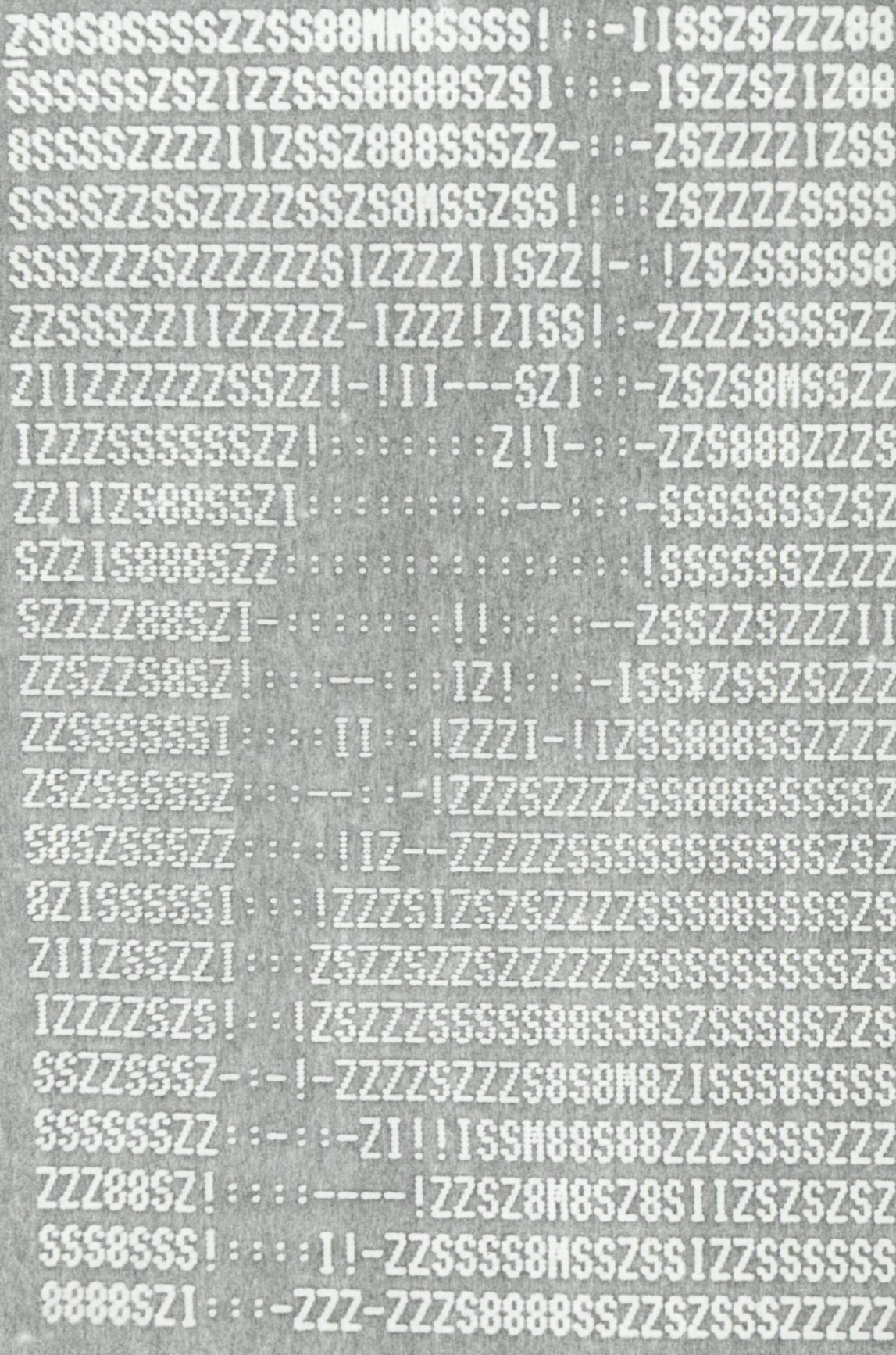

Figure 2 - Reduced Scale Digital Image Display

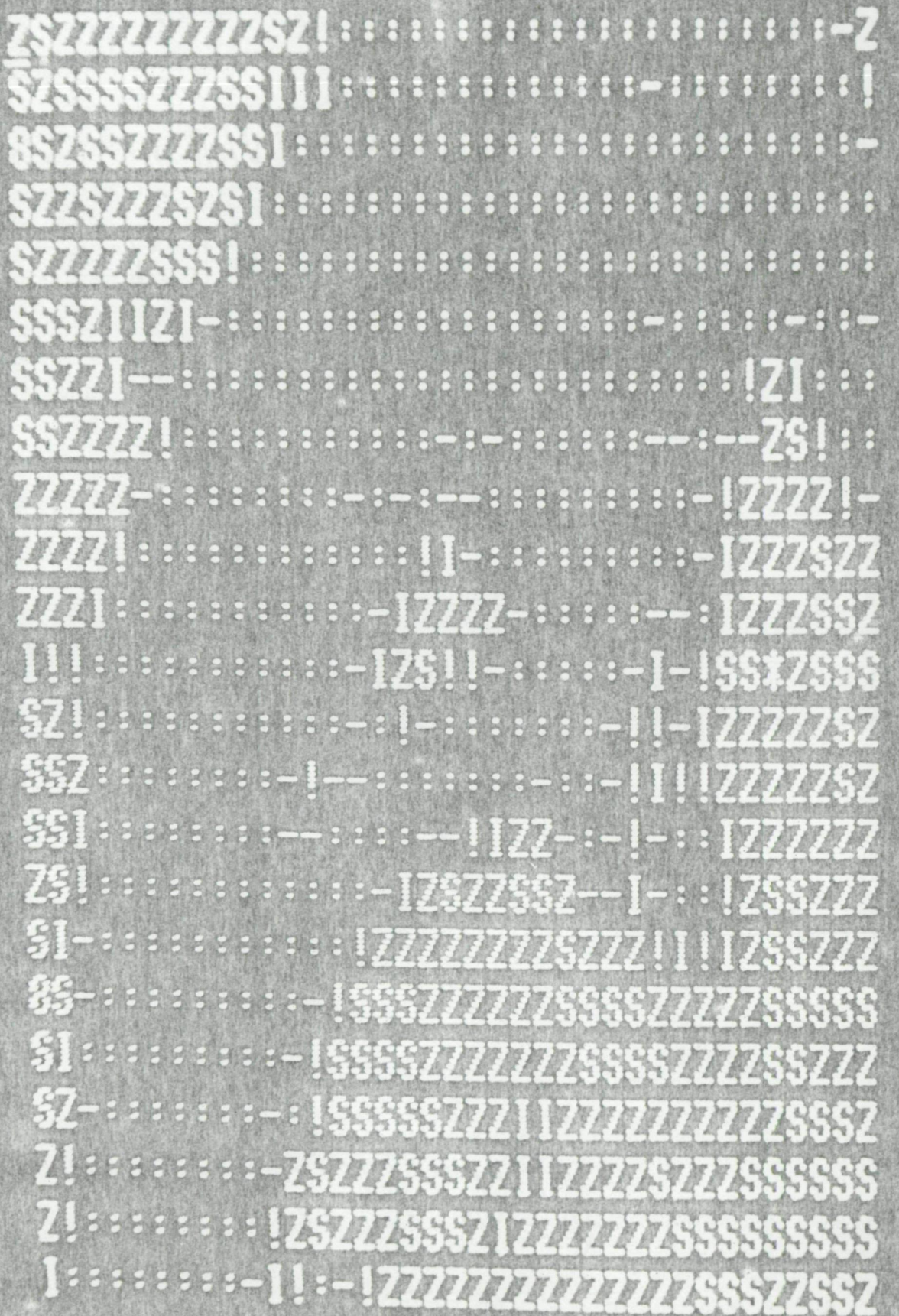

Figure 3 - Normal Scale Digital Image Display

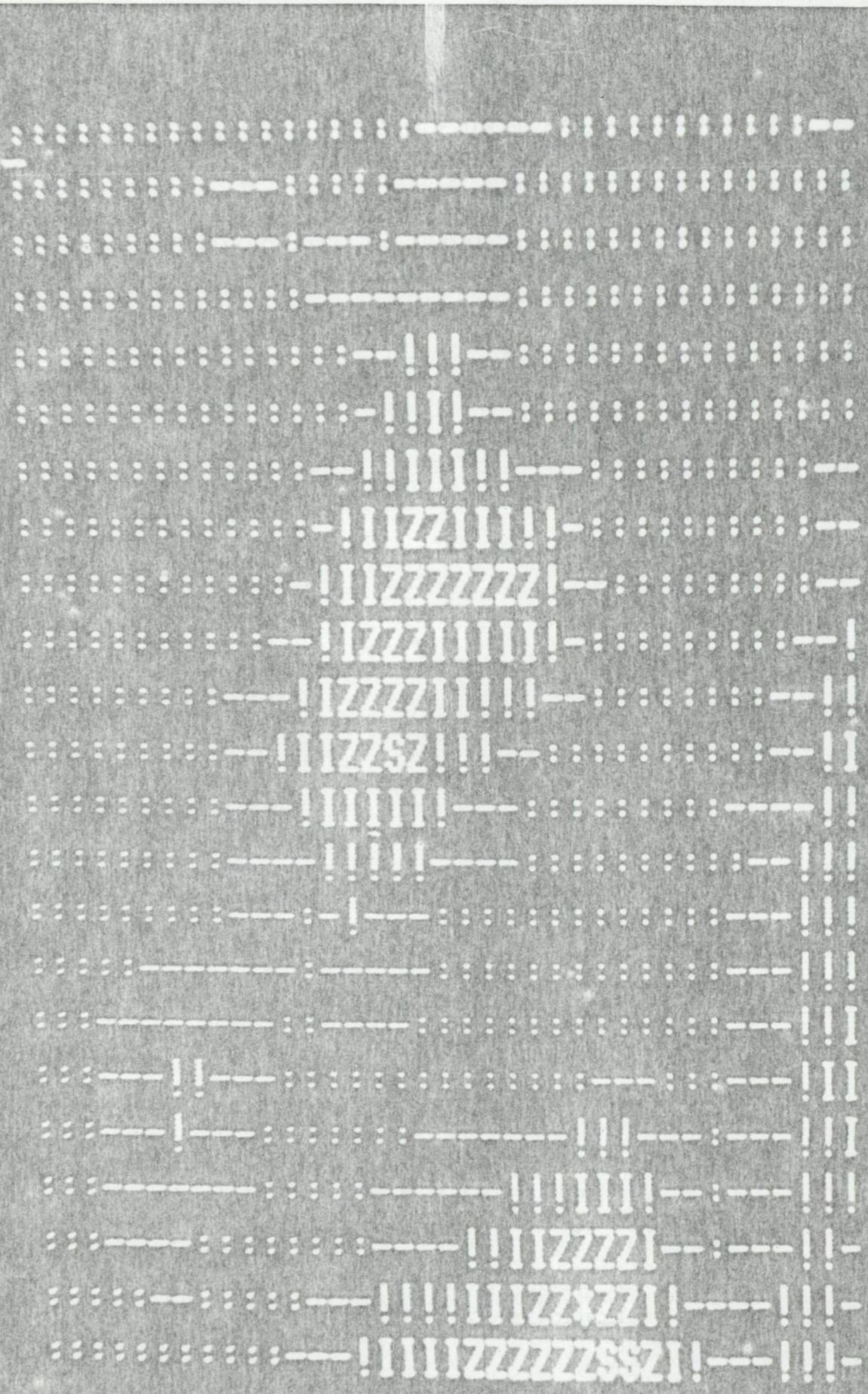

Figure 4 - Enlarged Scale Digital Image Display

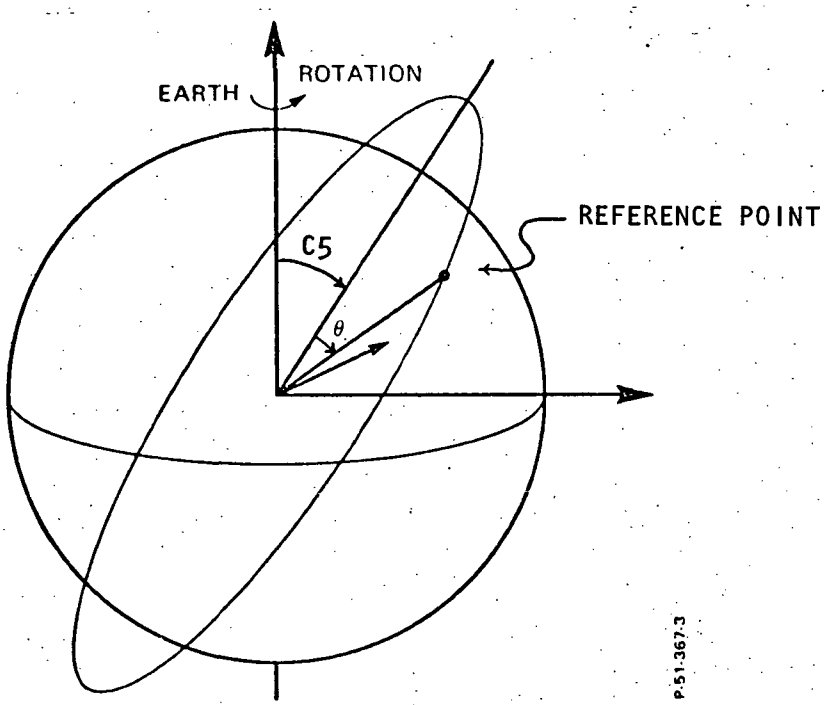

Figure 5 - Configuration of Spacecraft Orbit

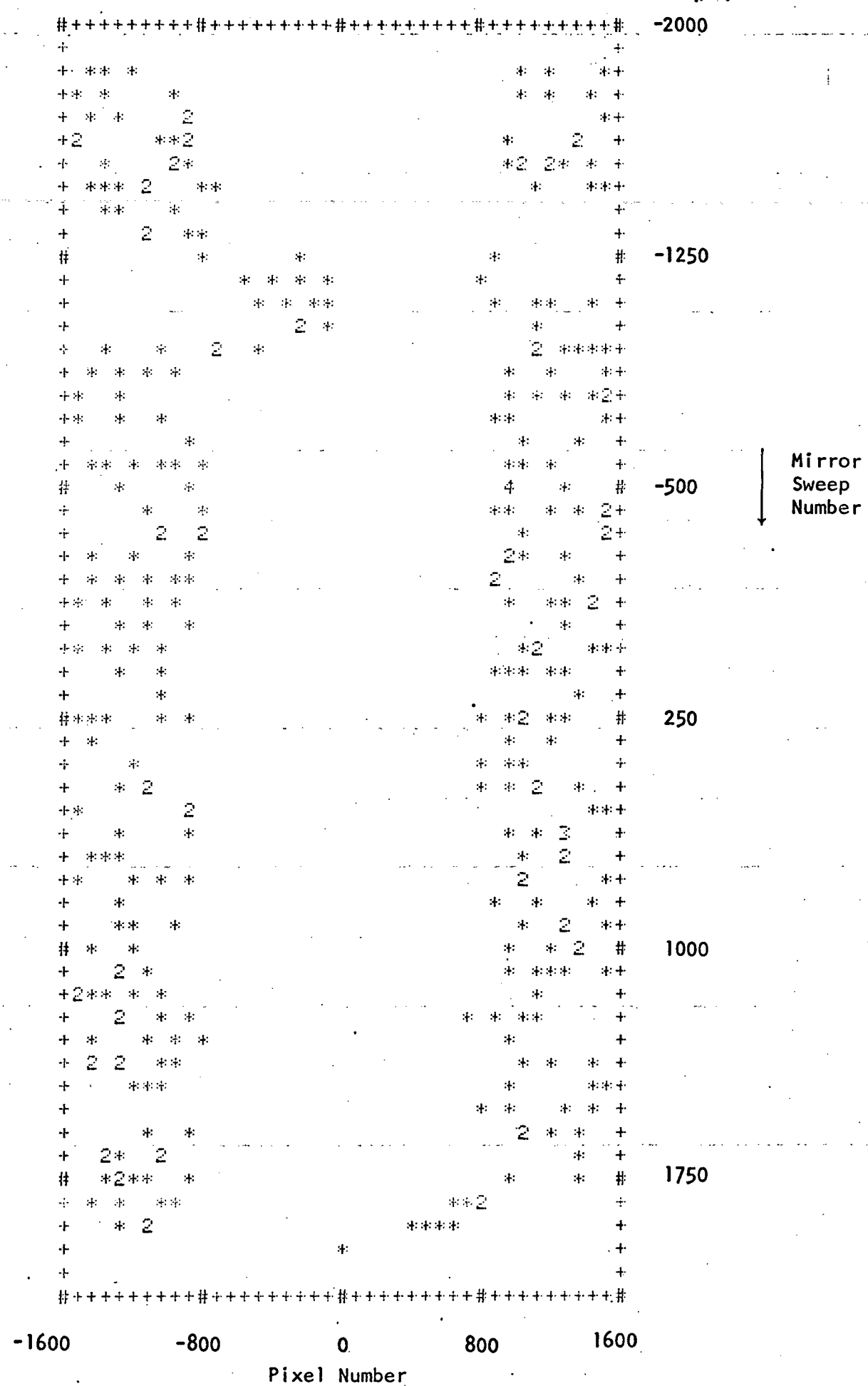

Figure 6 - Control Points Used for First Pass

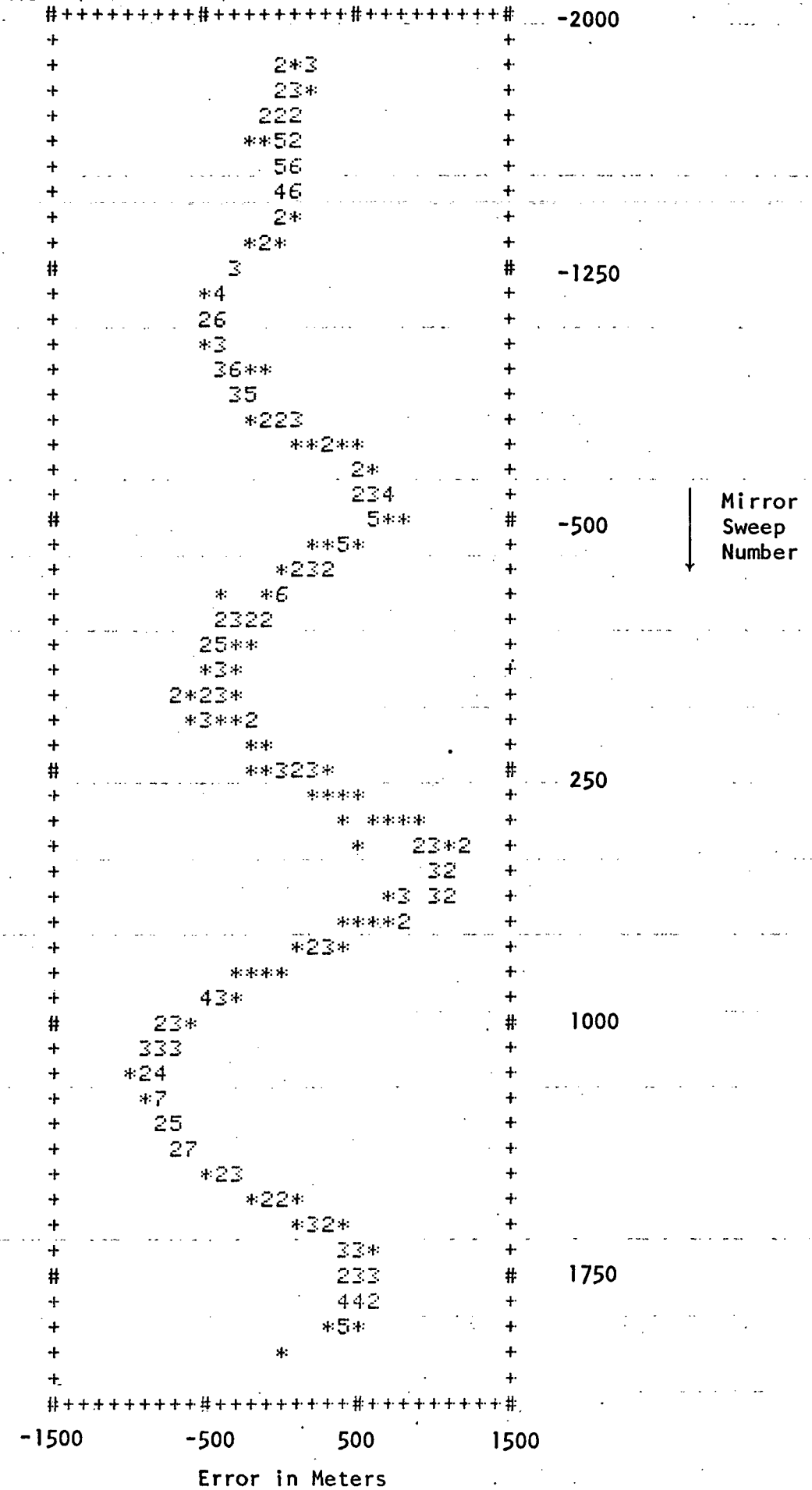

Figure 7 - First Pass Along Track Errors After Basic Model Determination

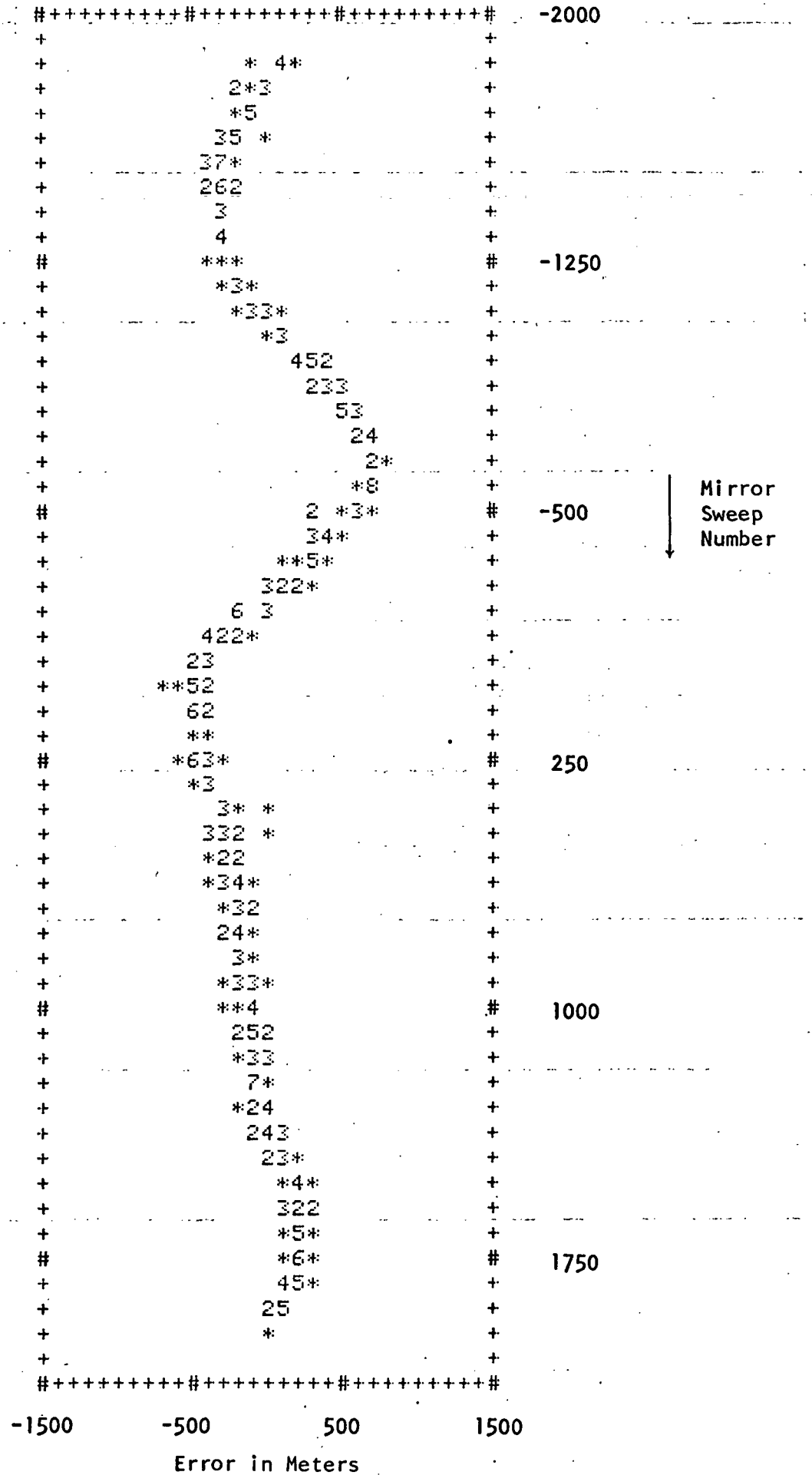

Figure 8 - First Pass Across Track Errors After Basic Model Determination

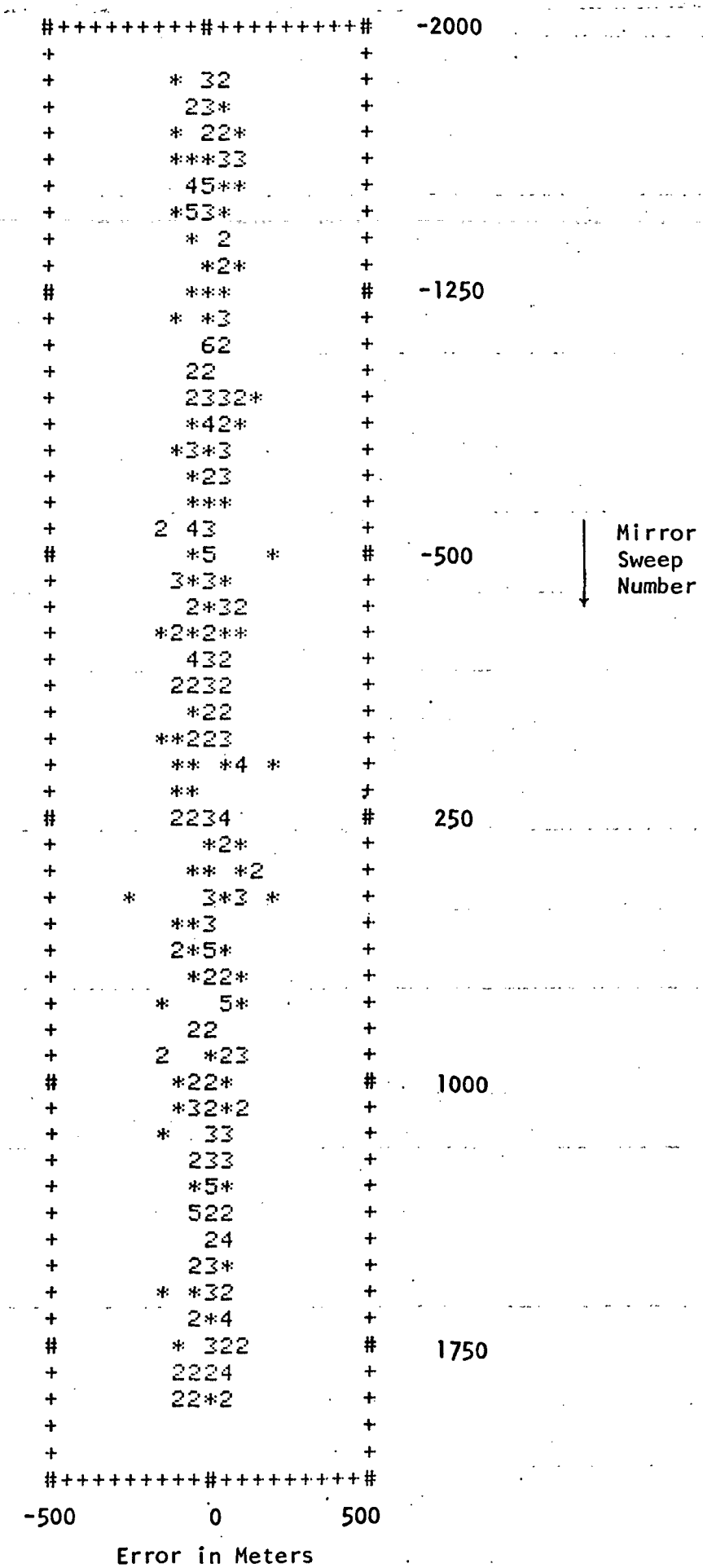

Figure 9 - First Pass Residual Errors Along Track After Attitude Effect Removal

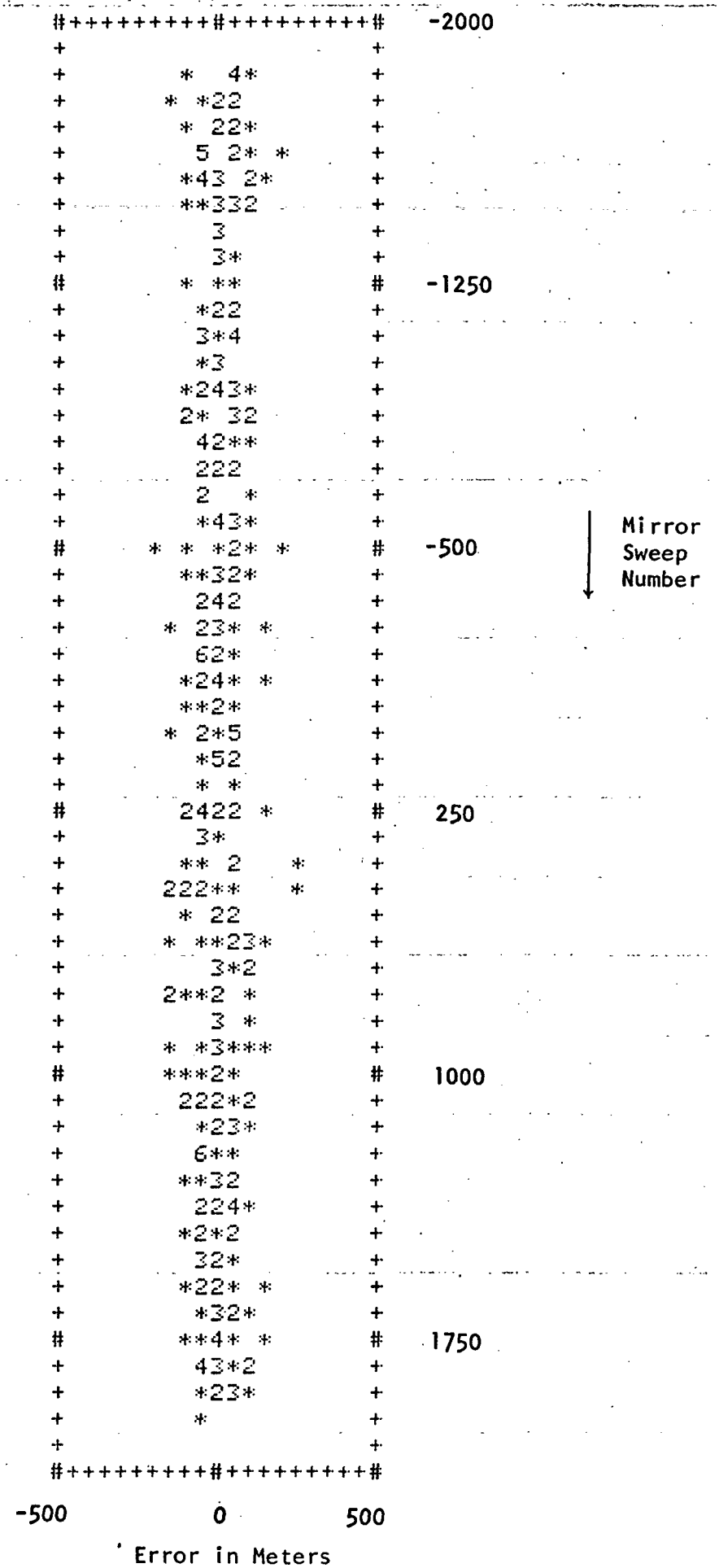

Figure 10 - First Pass Residual Errors Across Track After Attitude Effect Removal

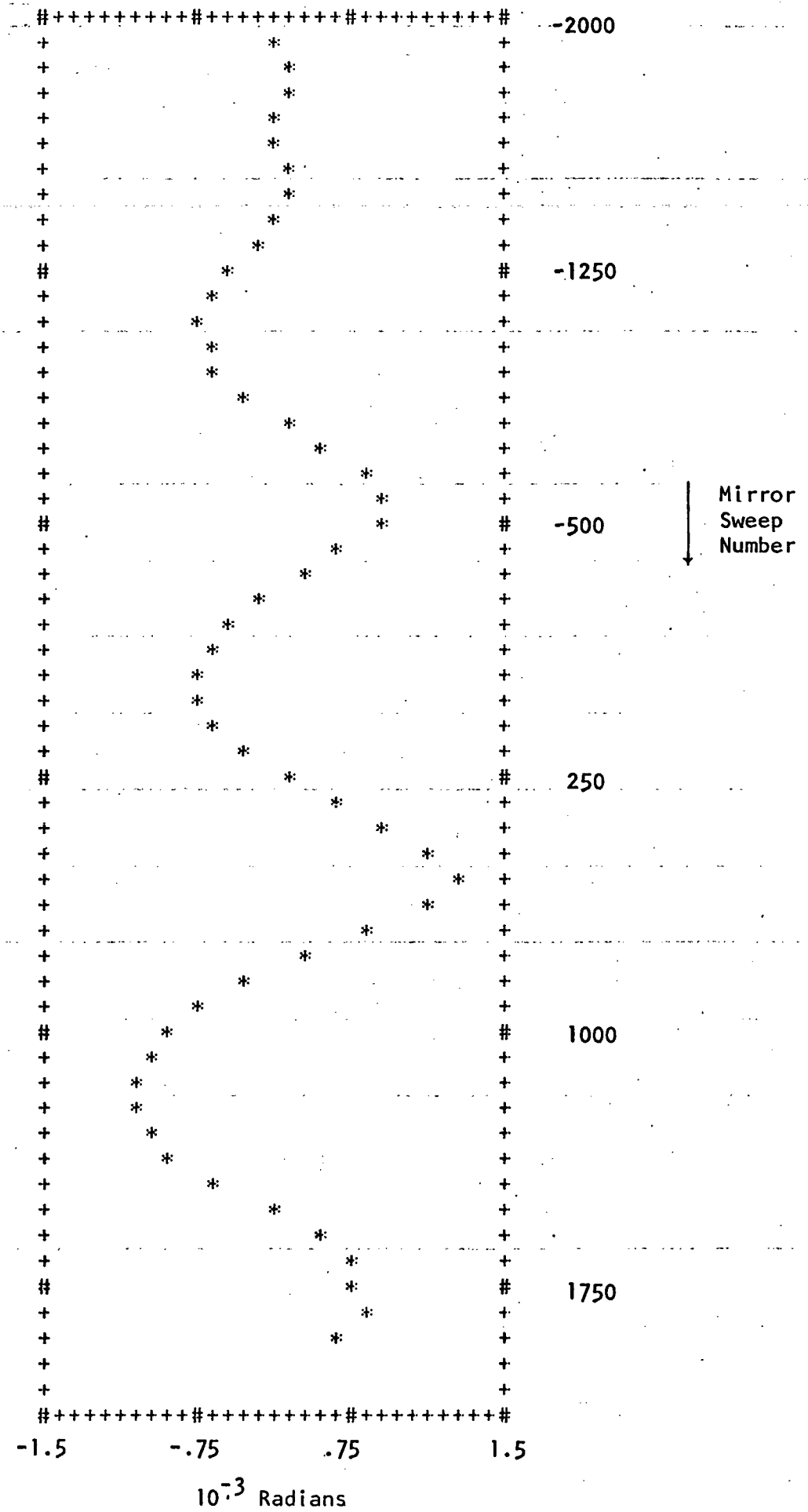

Figure 11 - First Pass Pitch Function

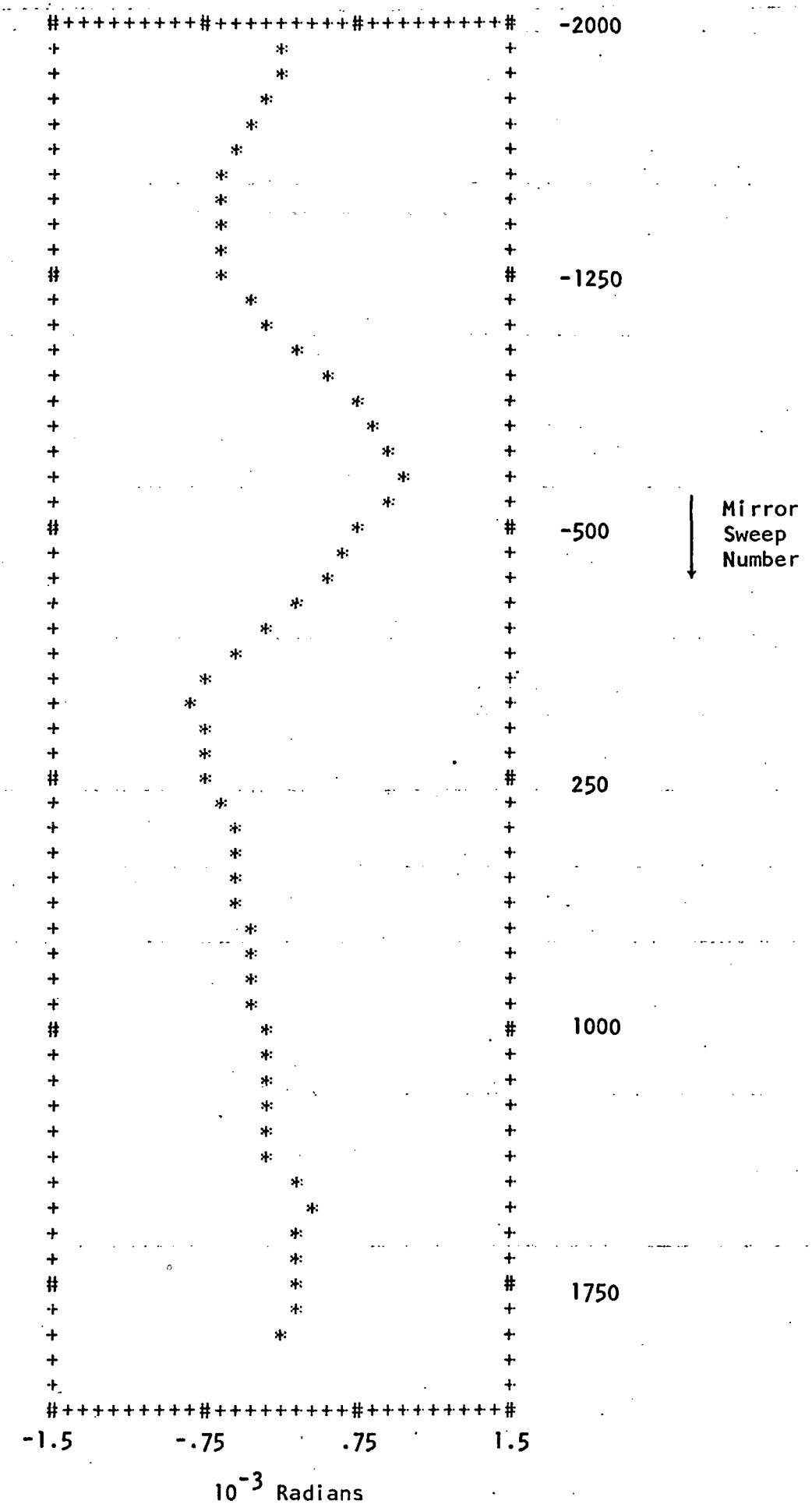

Figure 12 - First Pass Roll Function

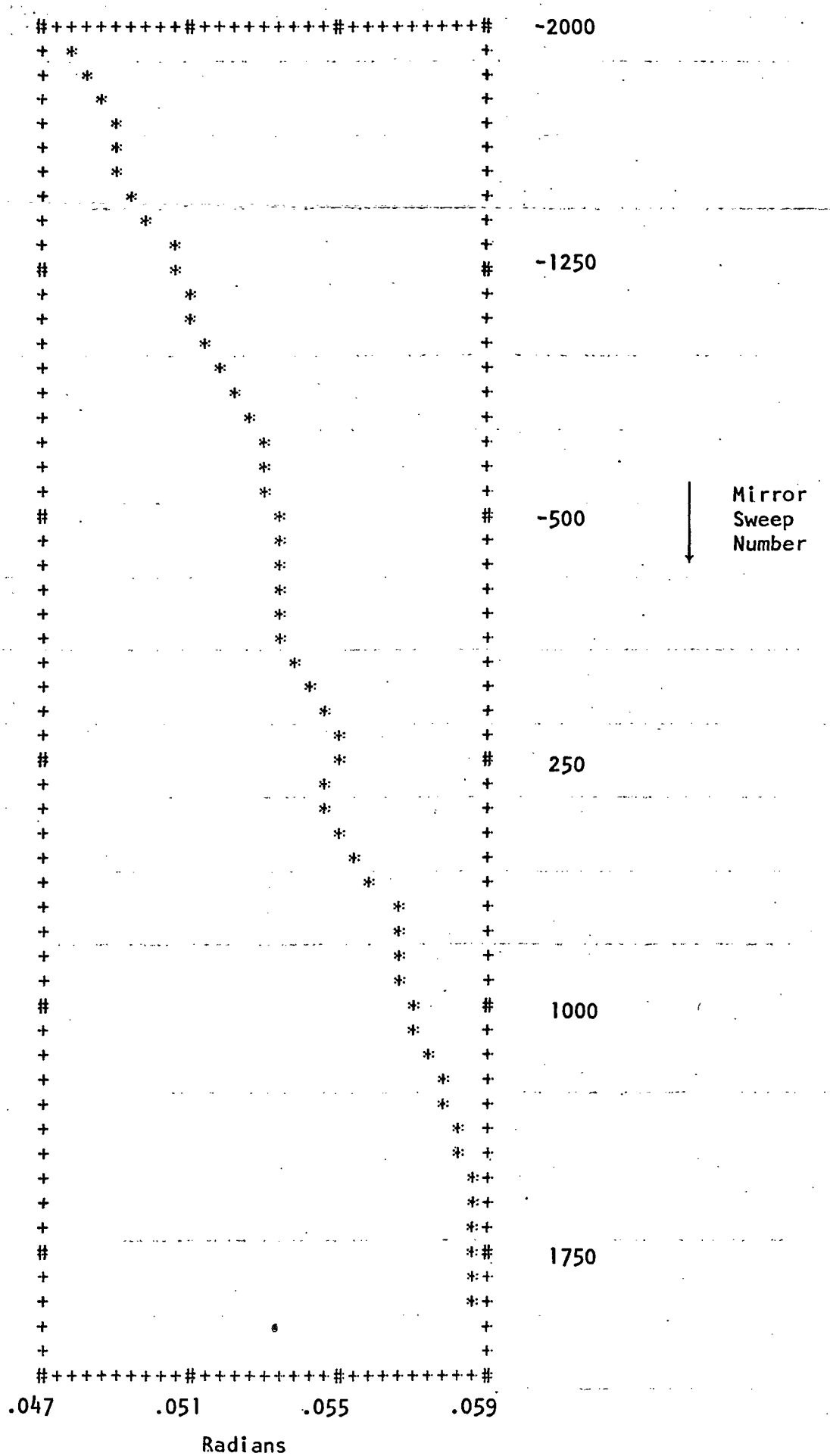

Figure 13 - First Pass Yaw Function

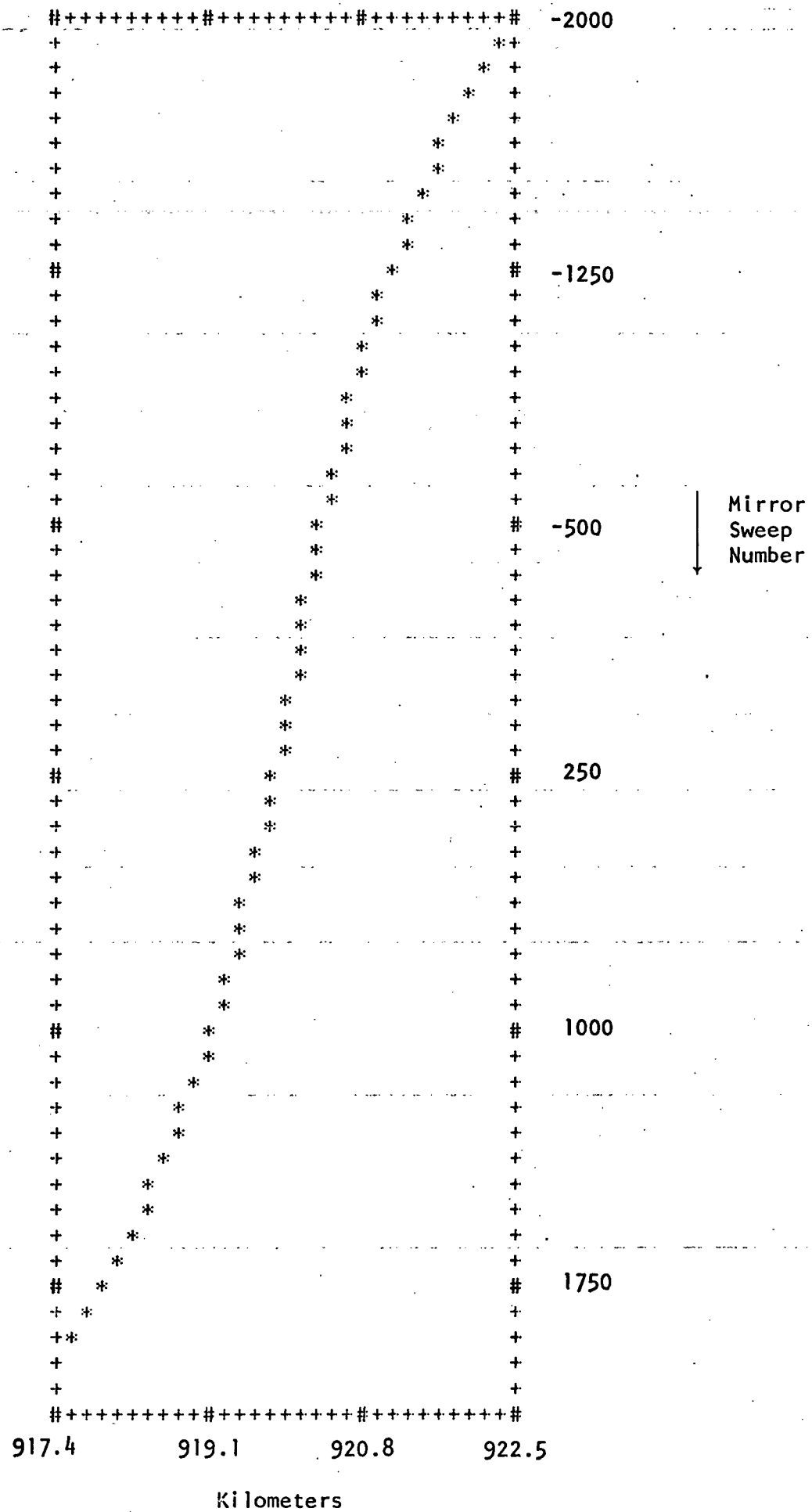

Figure 14 - First Pass Spacecraft Elevation

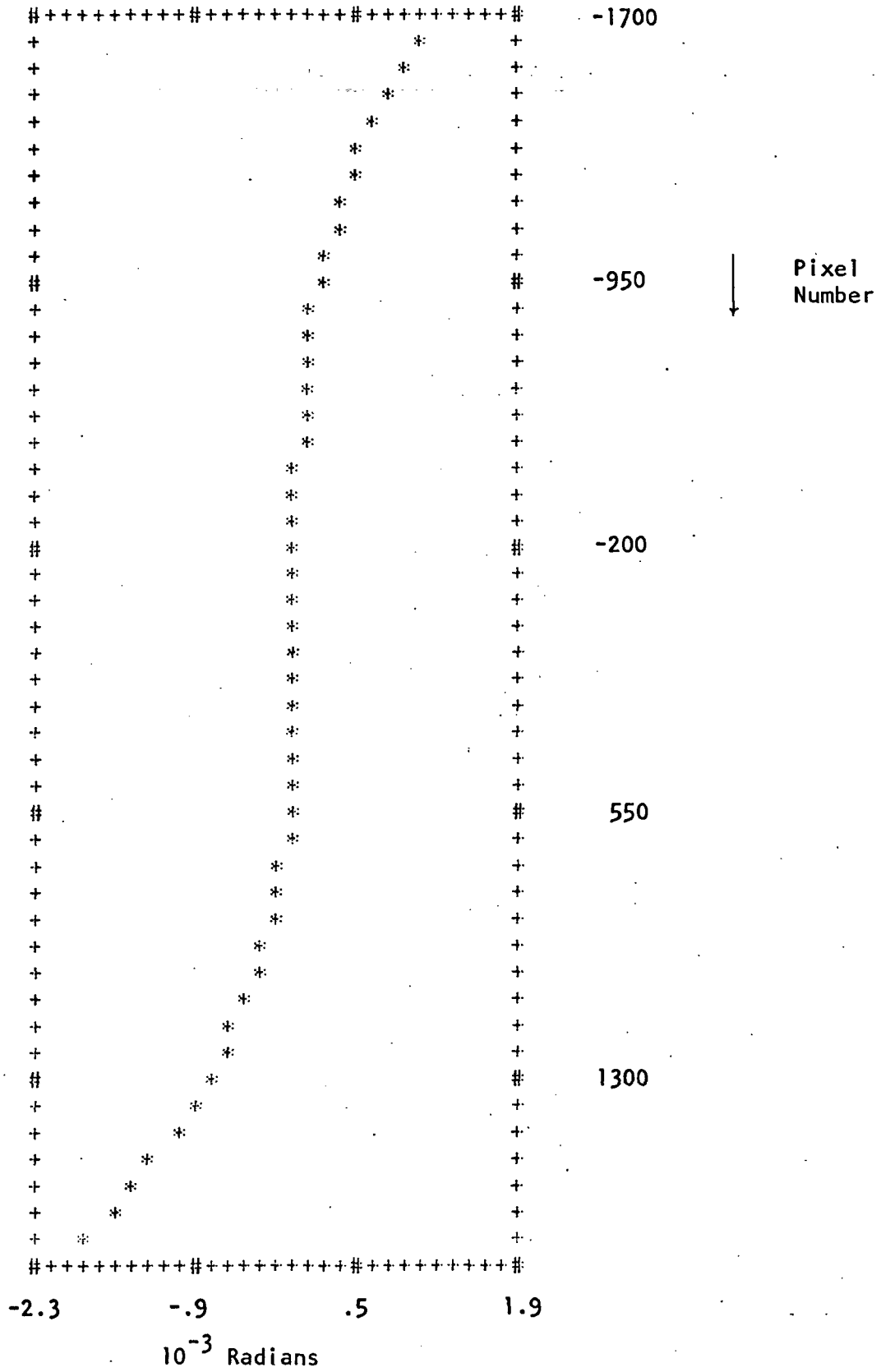

Figure 15 - First Pass Mirror Velocity Nonlinearity

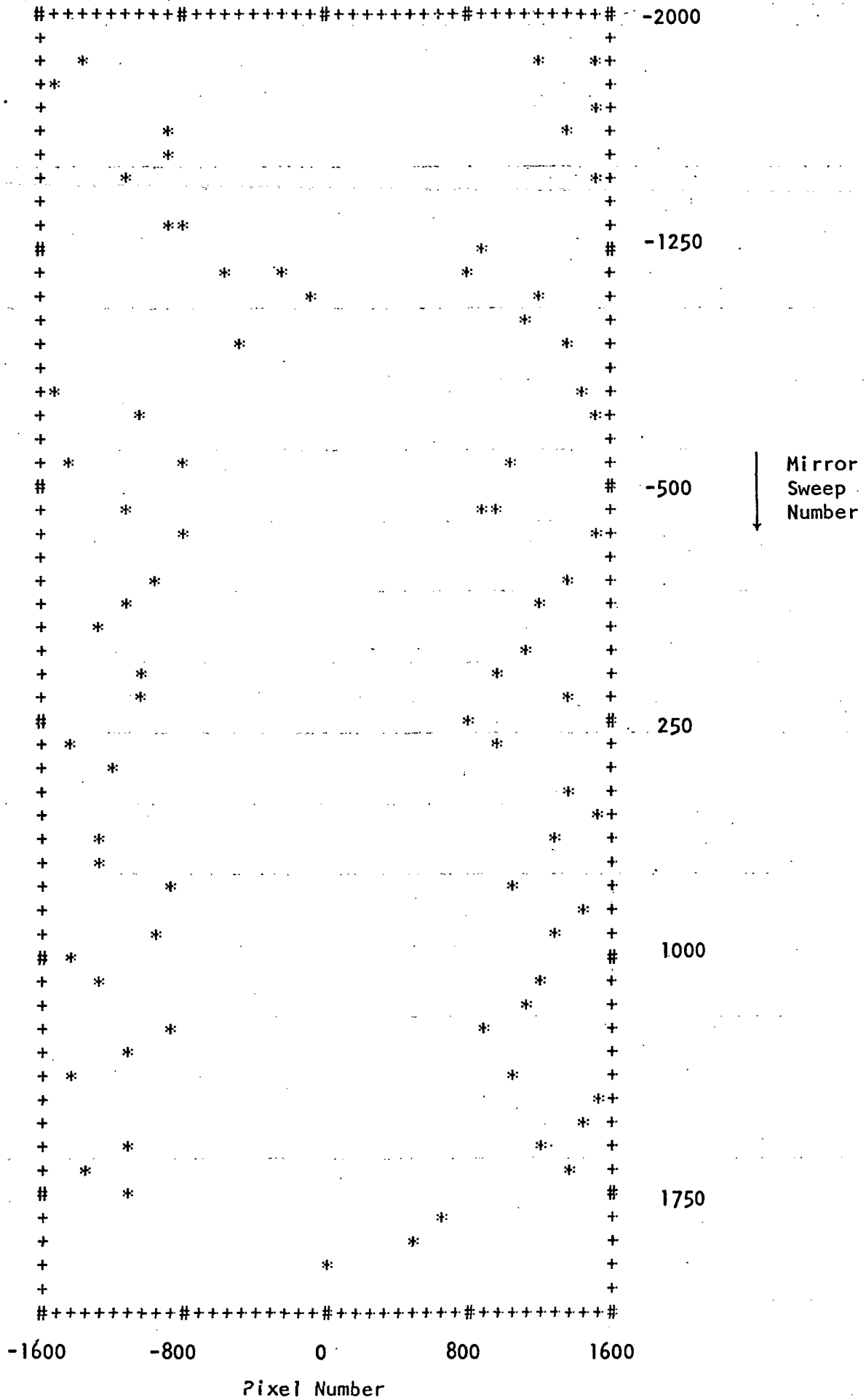

Figure 16 - Control Points Used for First Pass, 50 Mirror Sweep Spacing, Subset

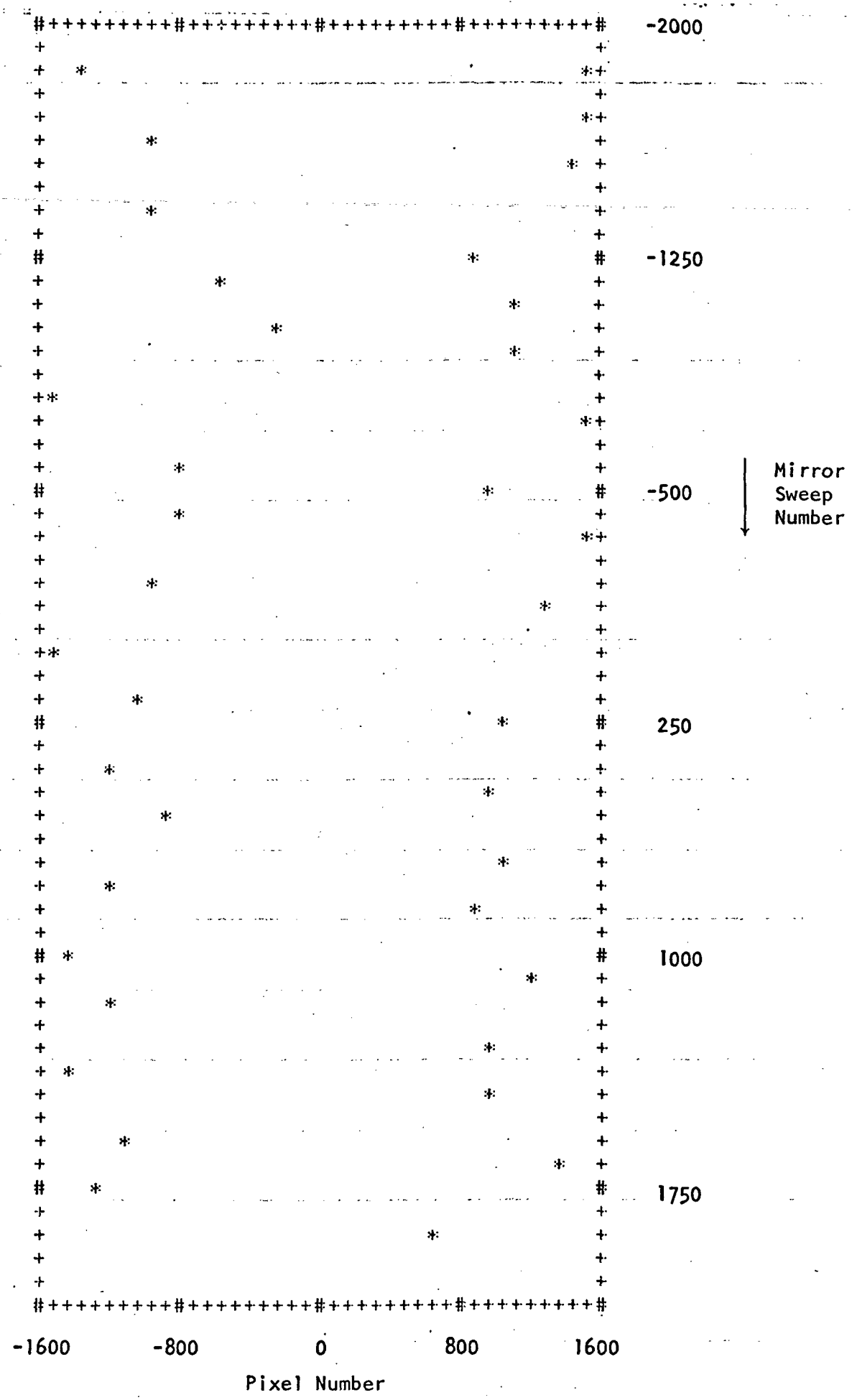

Figure 17 - Control Points Used for First Pass, 100 Mirror Sweep Spacing, Subset

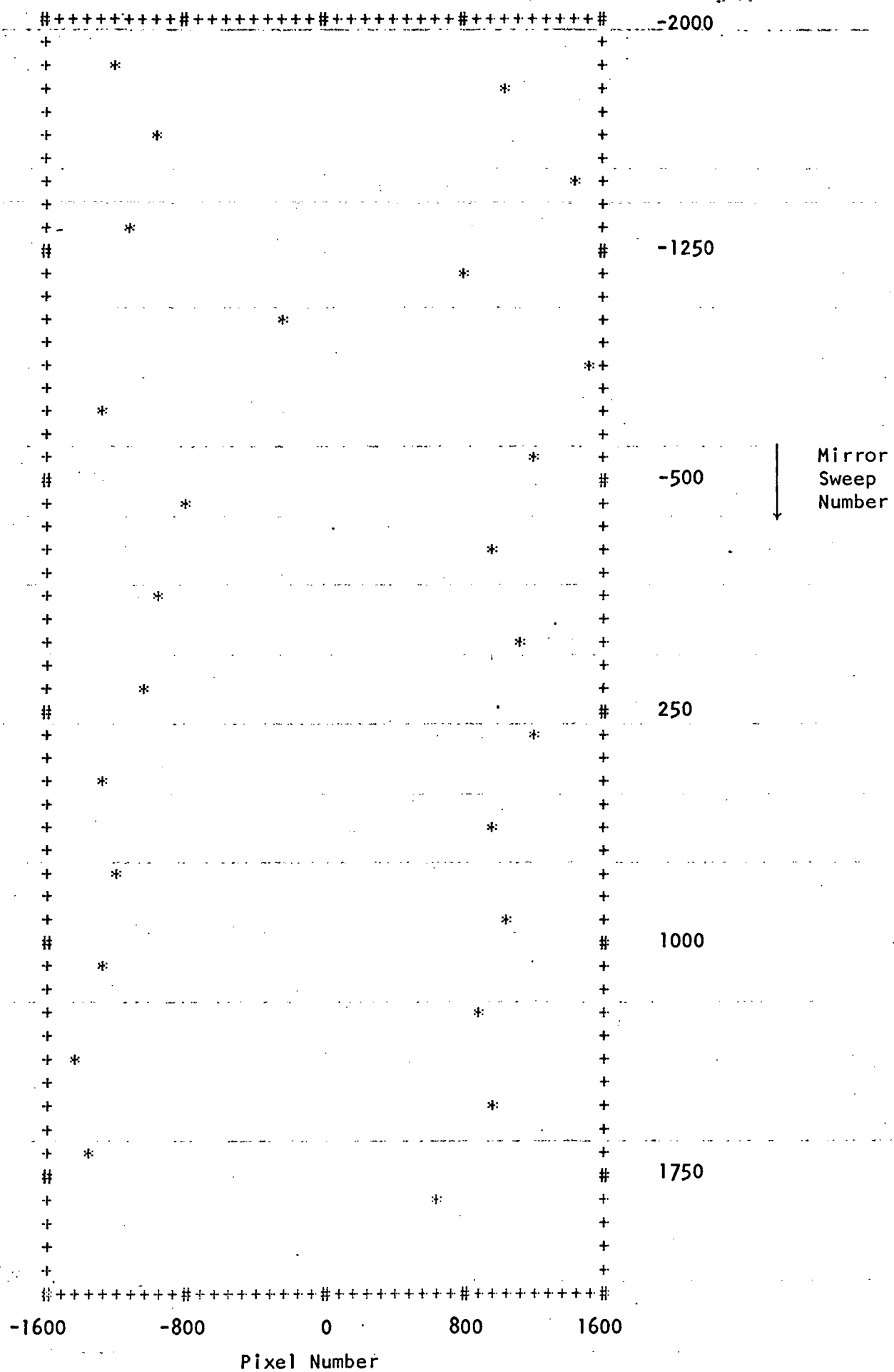

Figure 18 - Control Points Used for First Pass,
150 Mirror Sweep Spacing, Subset

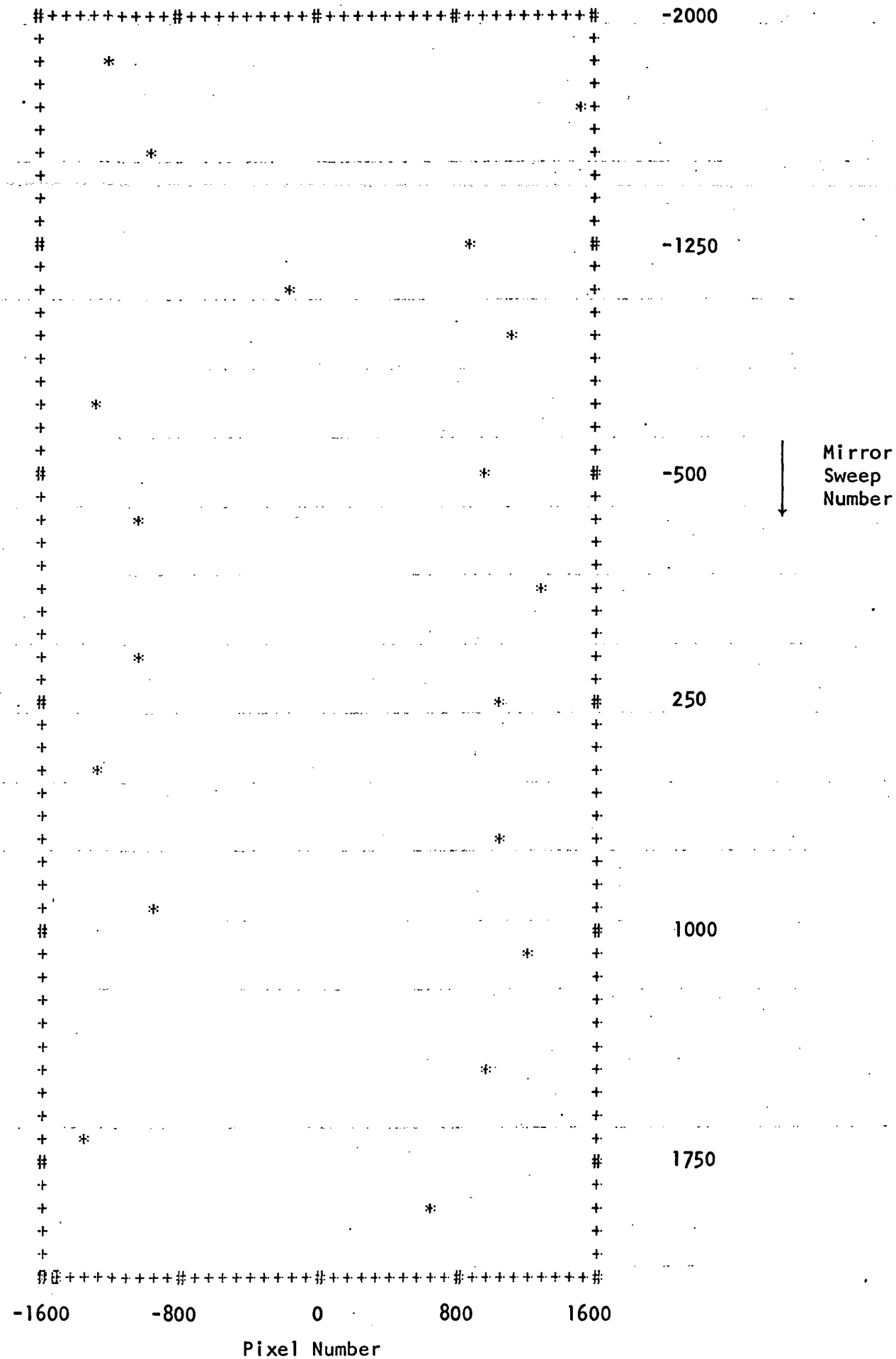

Figure 19 - Control Points Used for First Pass, 200 Mirror Sweep Spacing, Subset

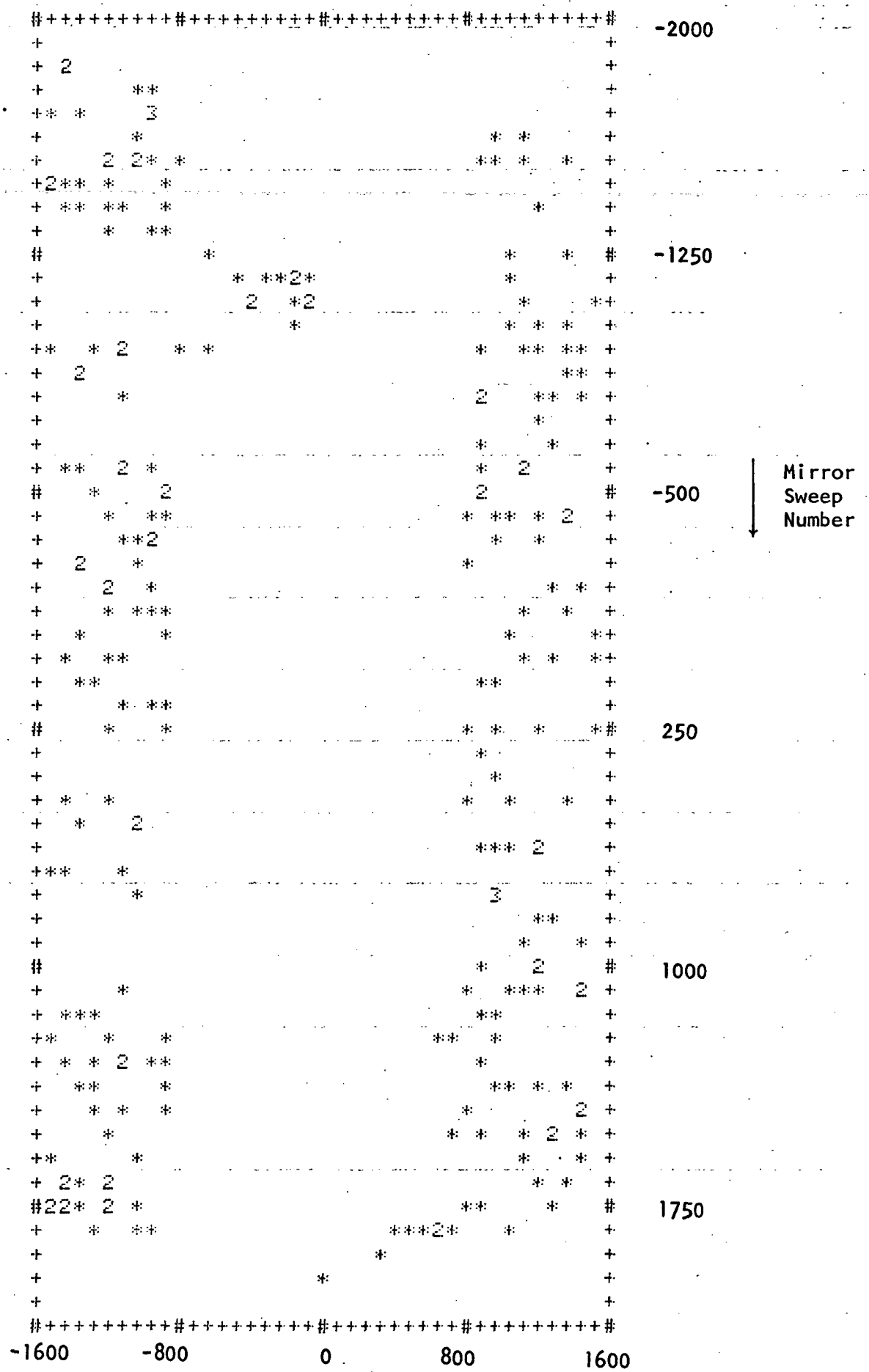

Figure 20 - Control Points Used for Second Pass

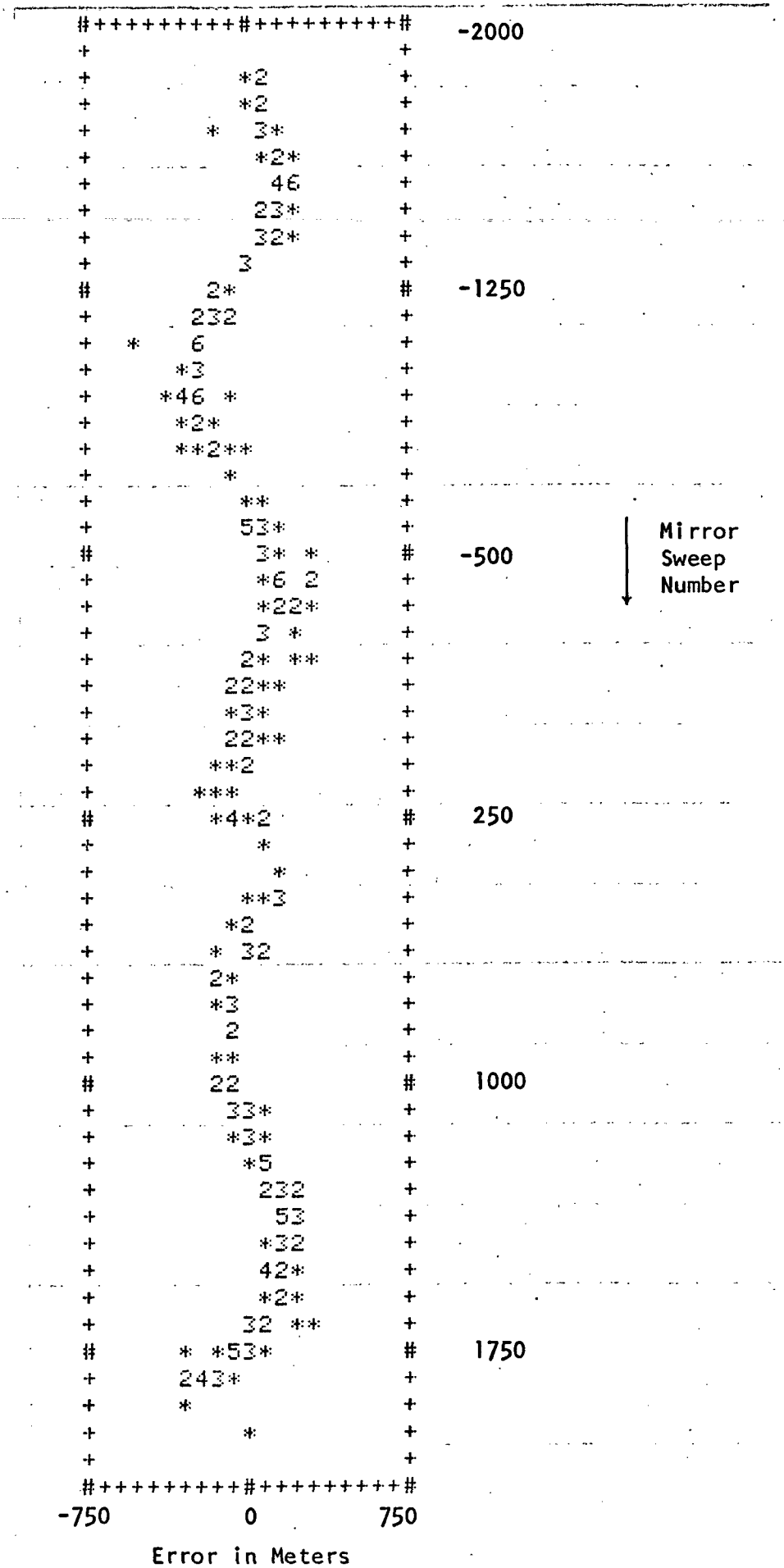

Figure 21 - Second Pass Along Track Errors After Basic Model Determination

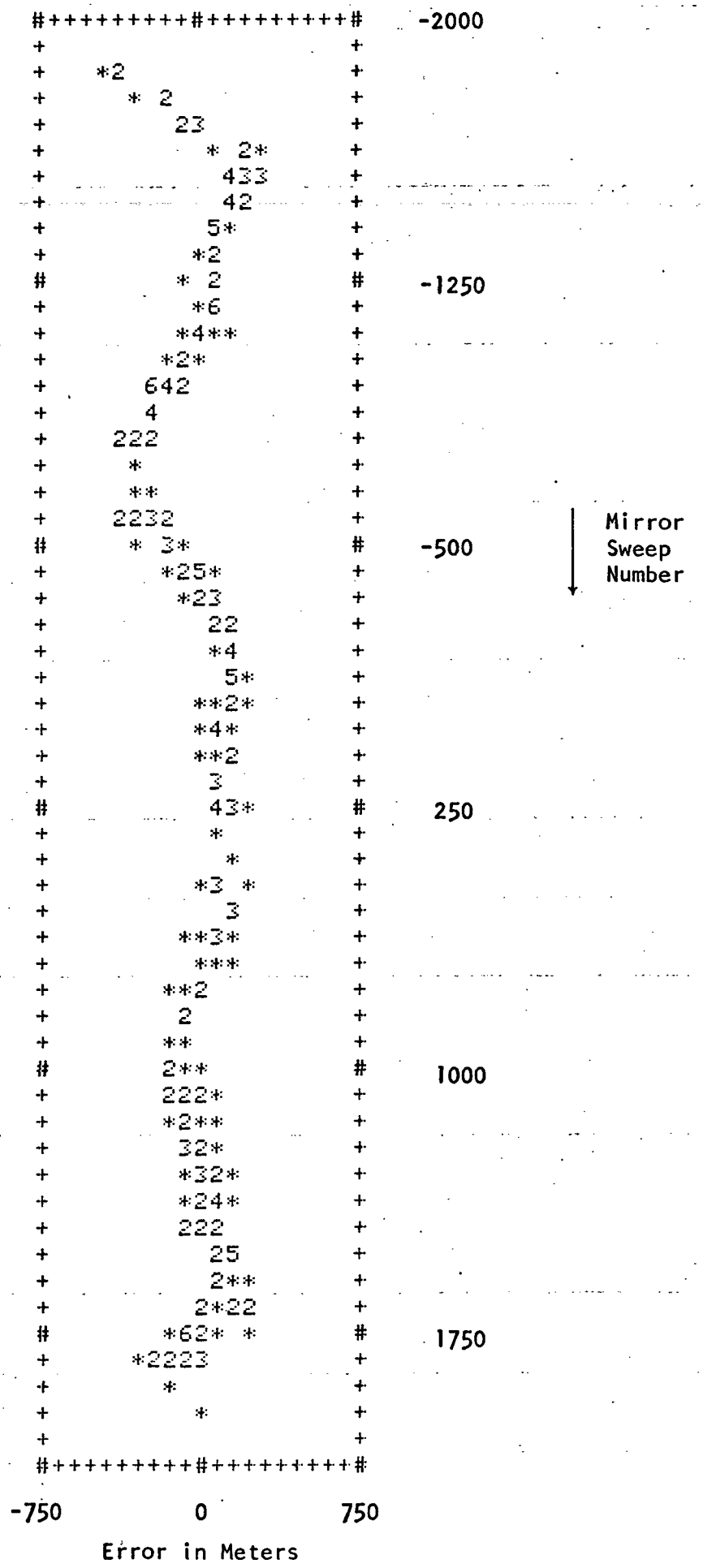

Figure 22 - Second Pass Across Track Errors After Basic Model Determination

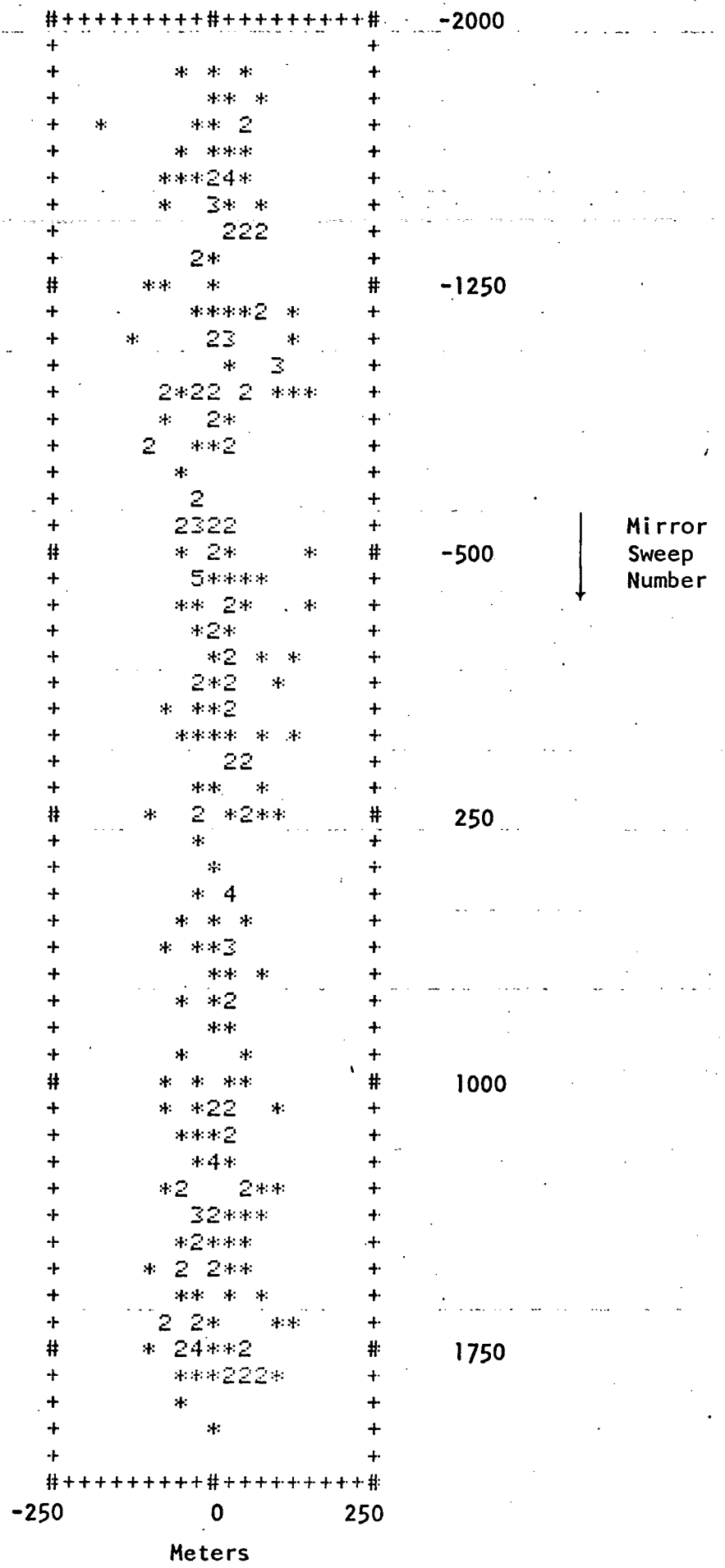

Figure 23 - Second Pass Residual Errors Along Track After Attitude Effect Removal

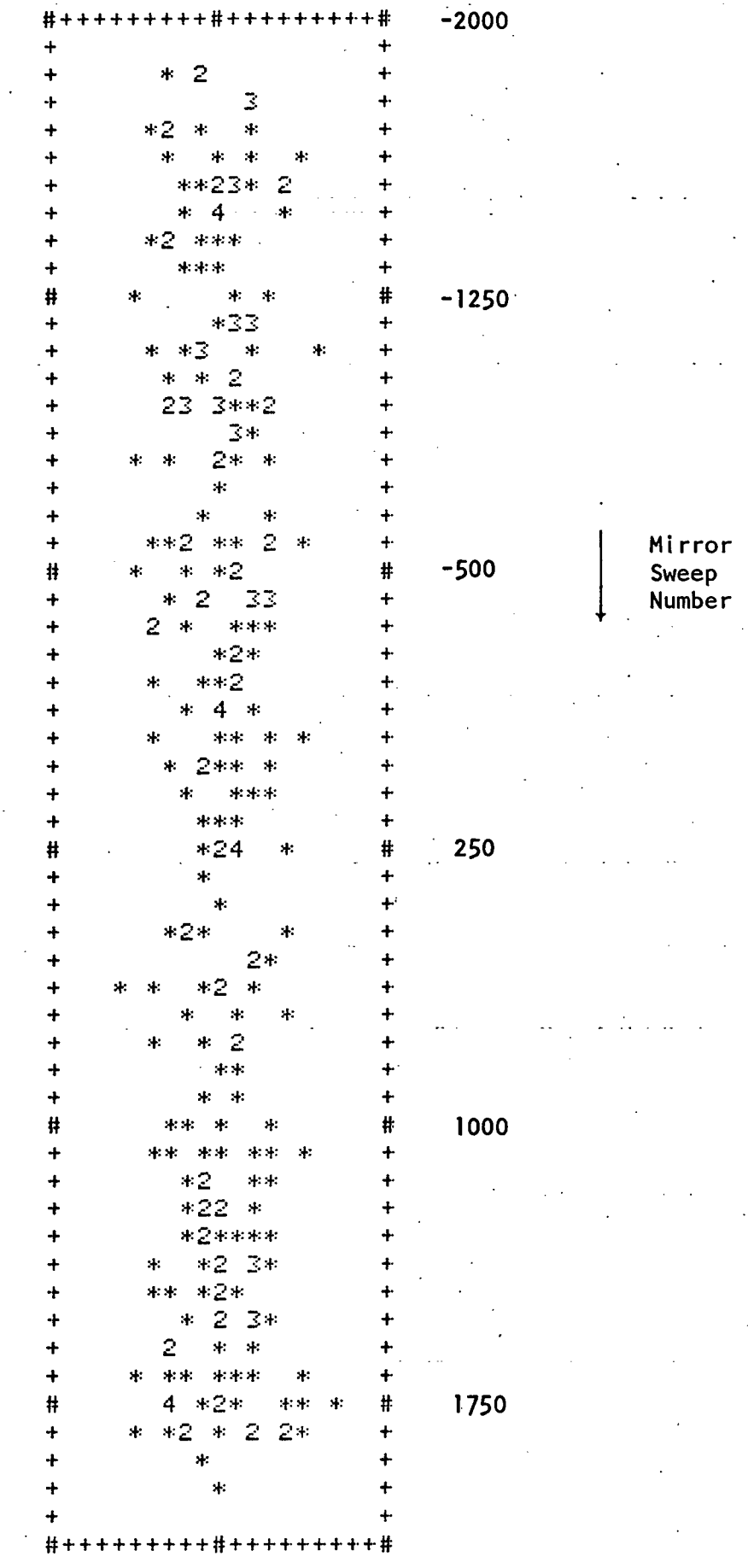

Figure 24 - Second Pass Residual Errors Across Track After Attitude Effect Removal

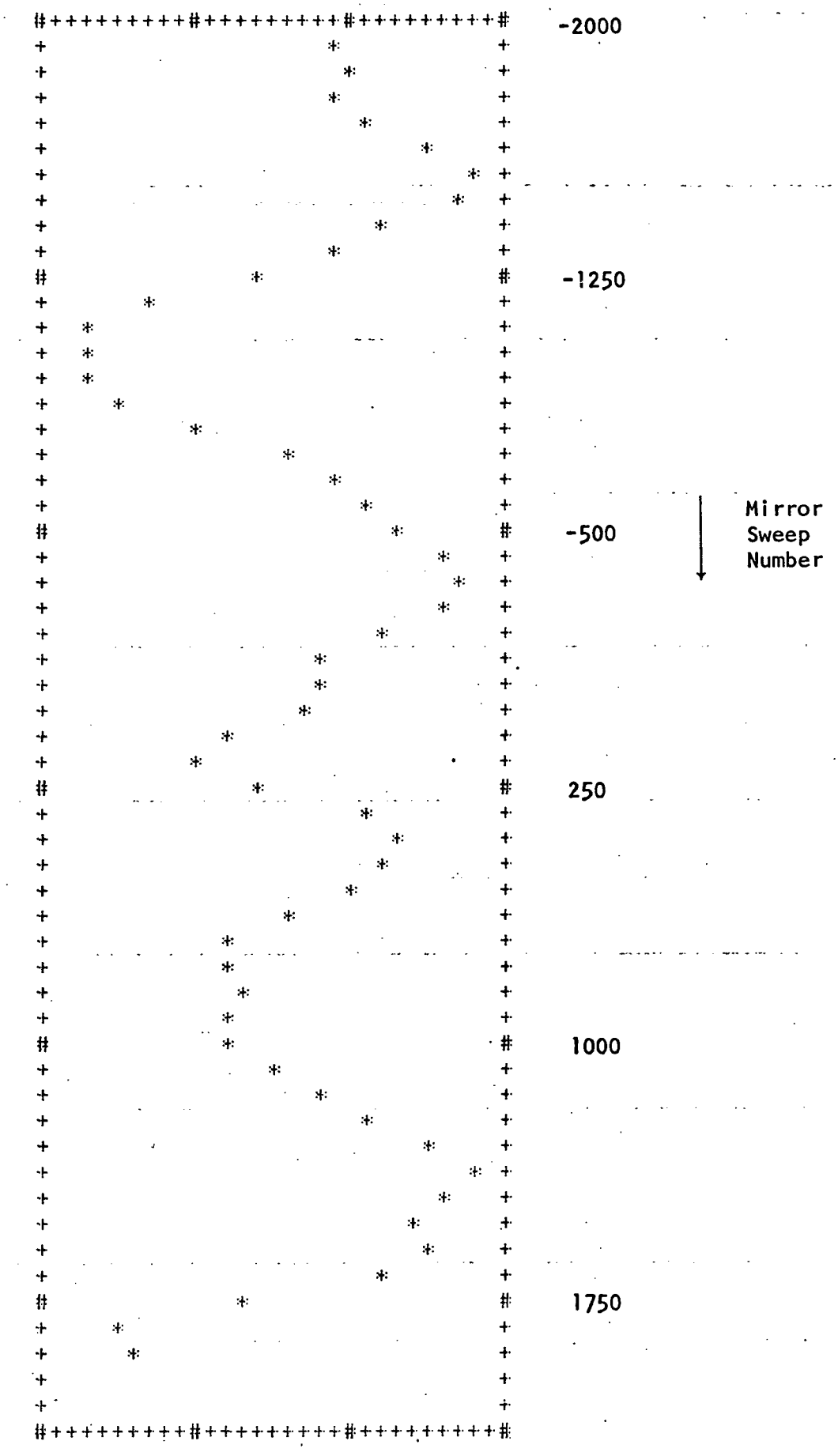

Figure 25 - Second Pass Pitch Function

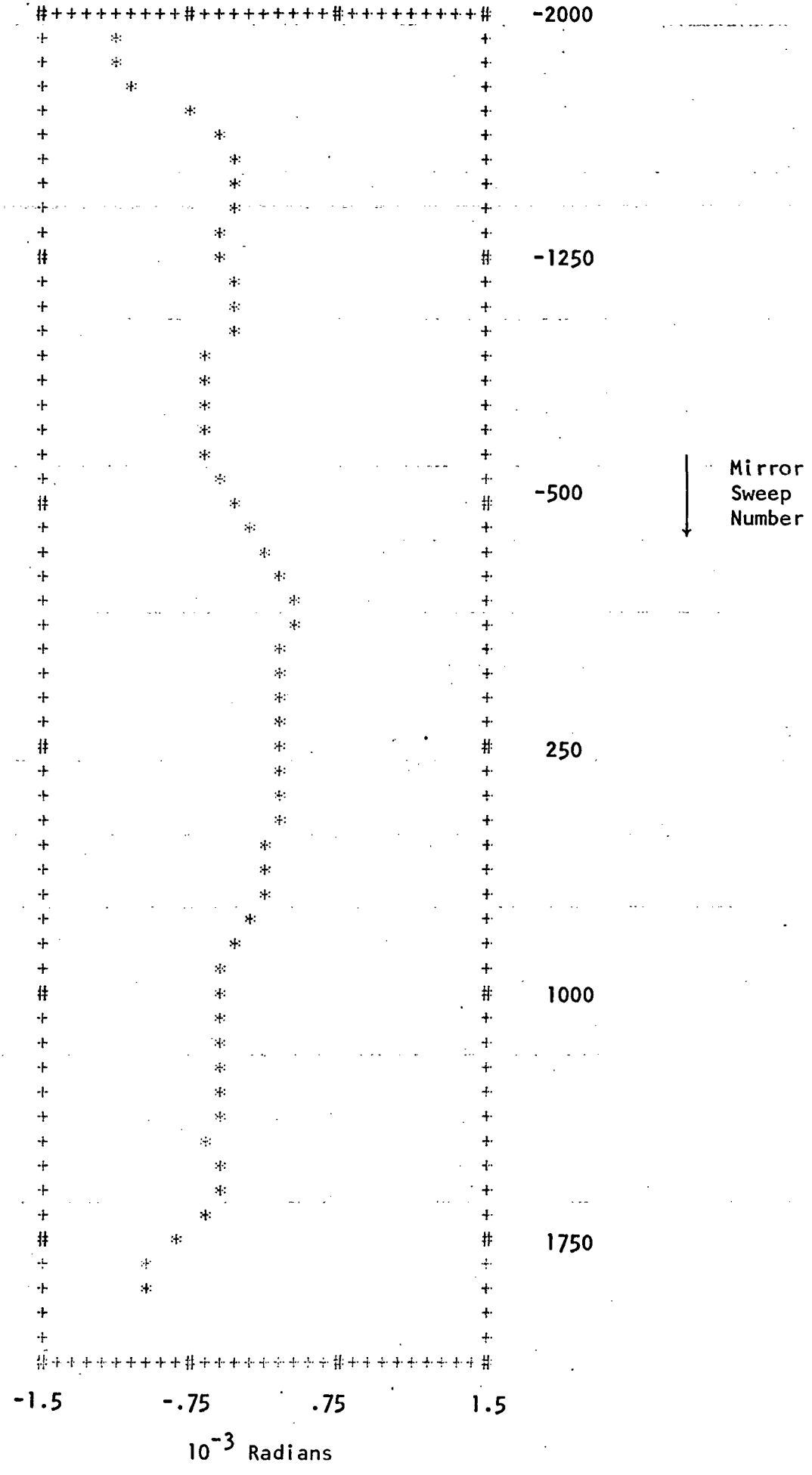

Figure 26 - Second Pass Roll Function

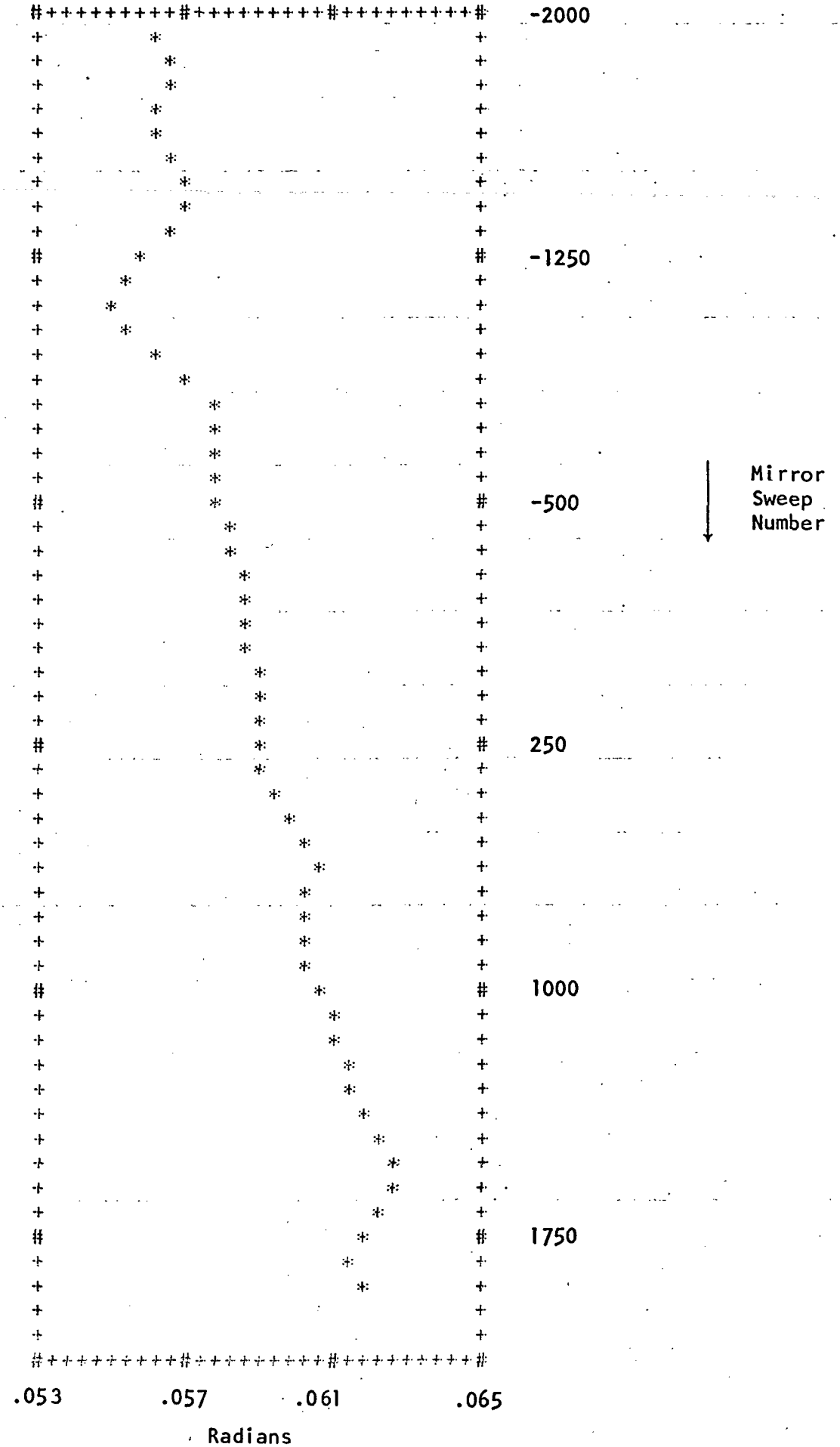

Figure 27 - Second Pass Yaw Function

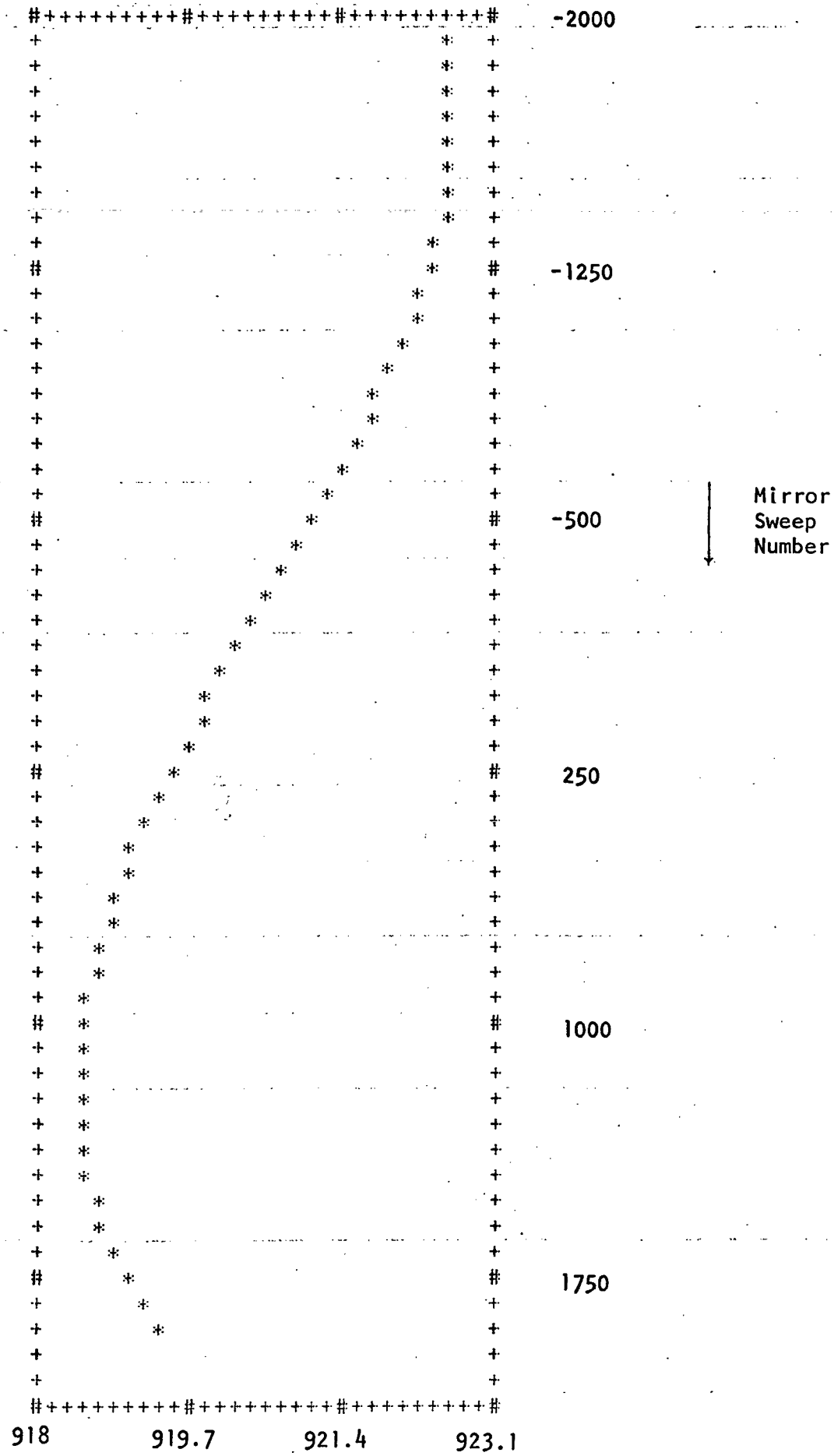

Figure 28 - Second Pass Spacecraft Elevation

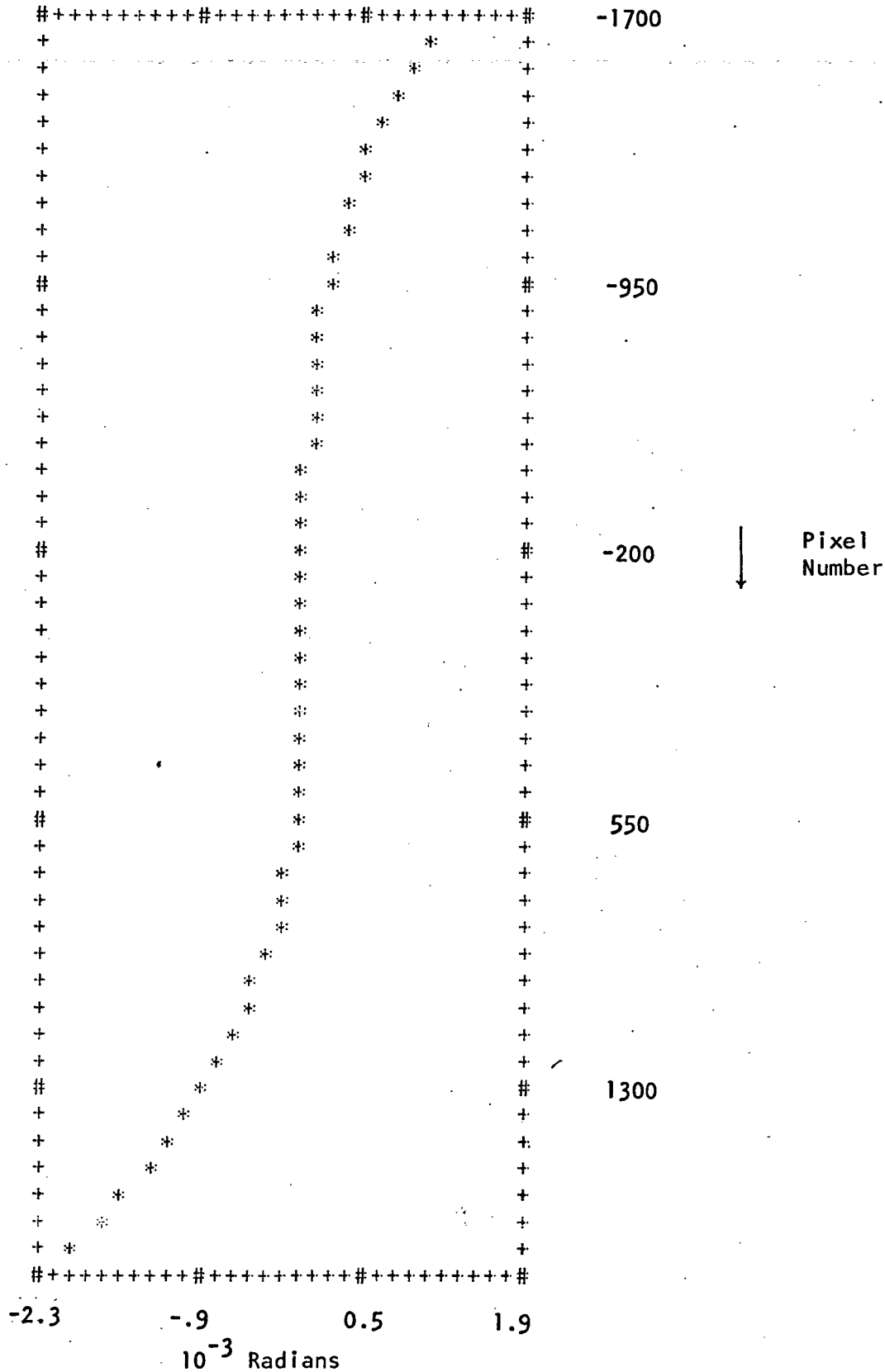

Figure 29 - Second Pass Mirror Velocity Nonlinearity

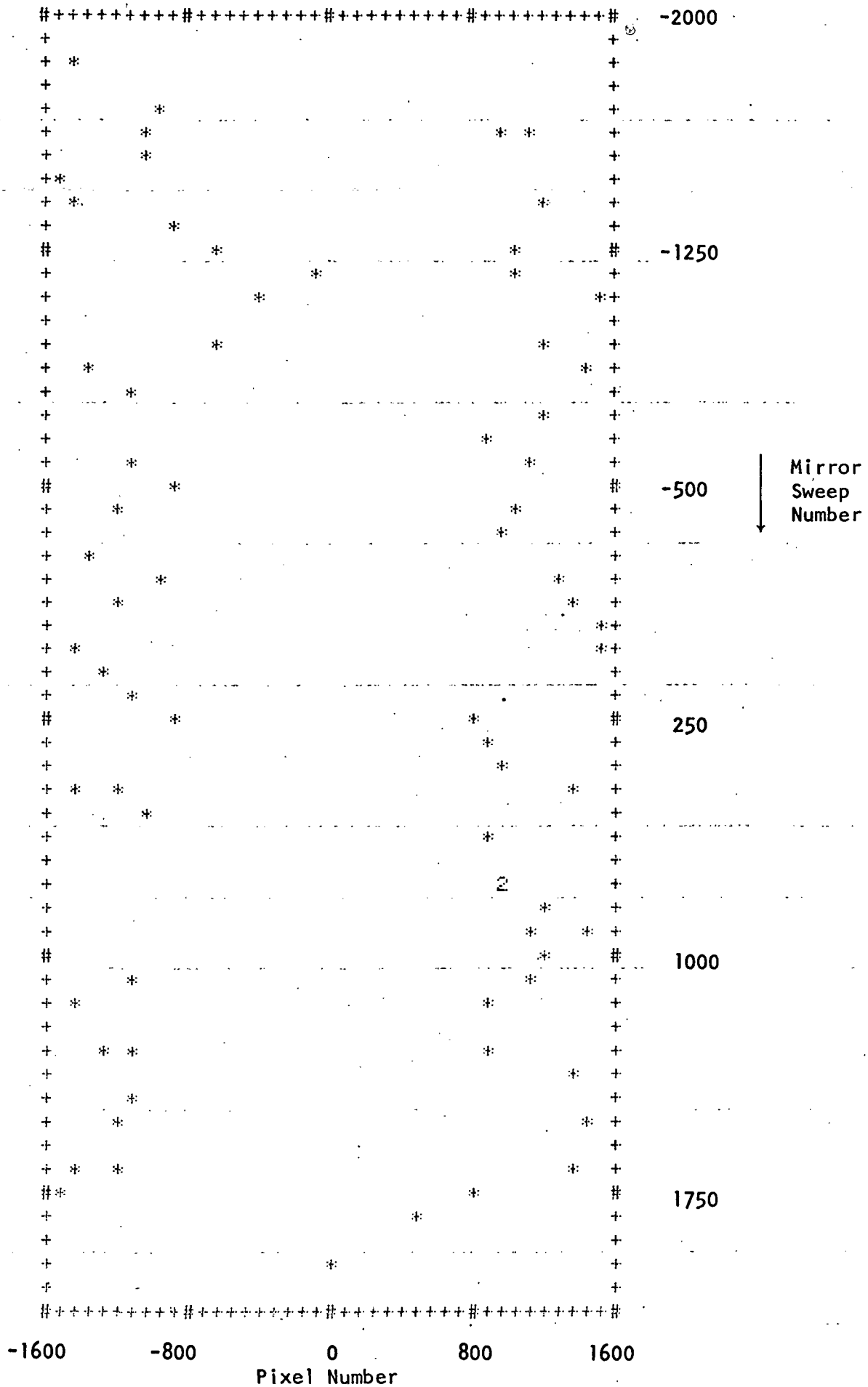

Figure 30 - Control Points Used for Second Pass, 50 Mirror Sweep Spacing, Subset

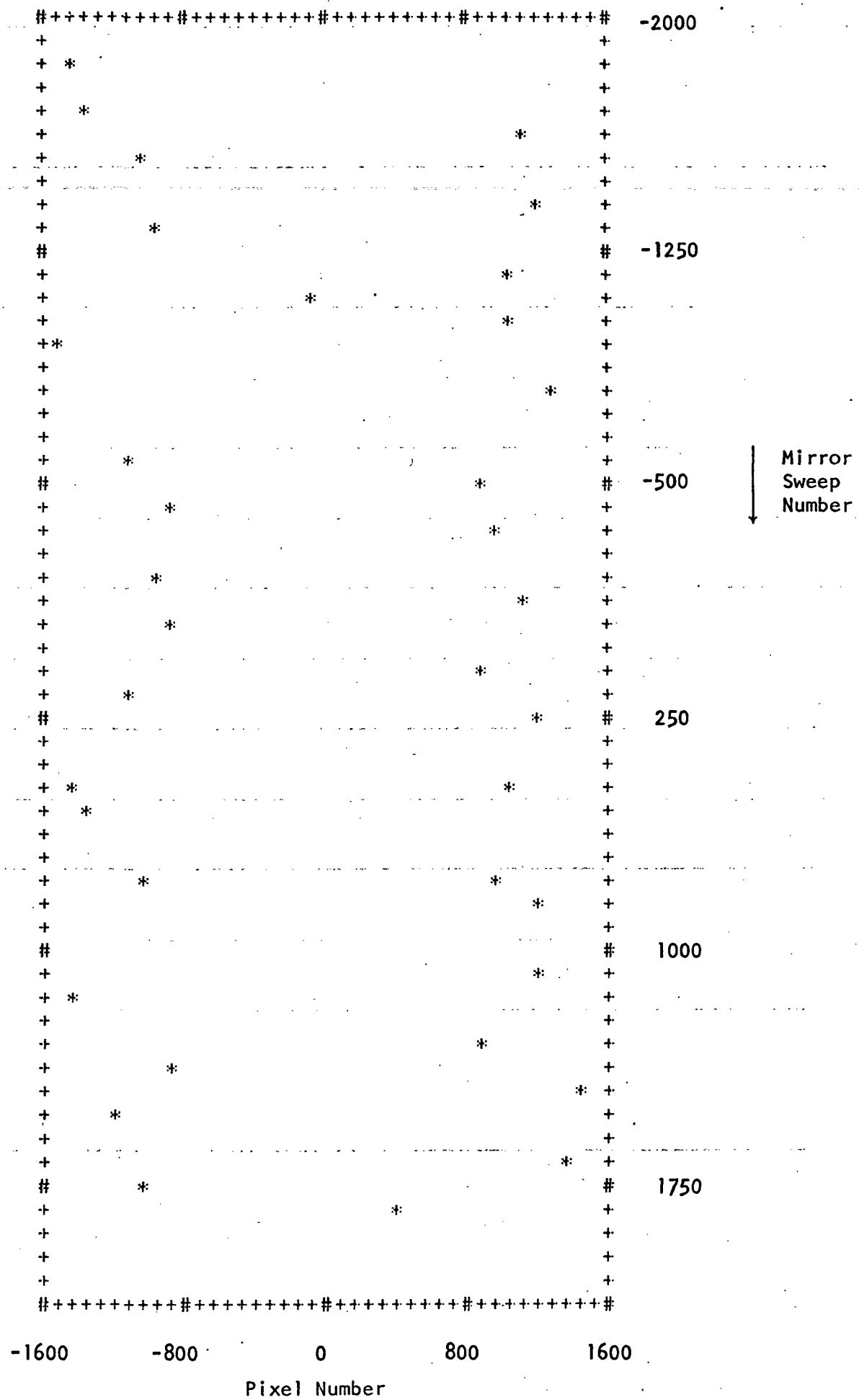

Figure 31 - Control Points Used for Second Pass
100 Mirror Sweep Spacing, Subset

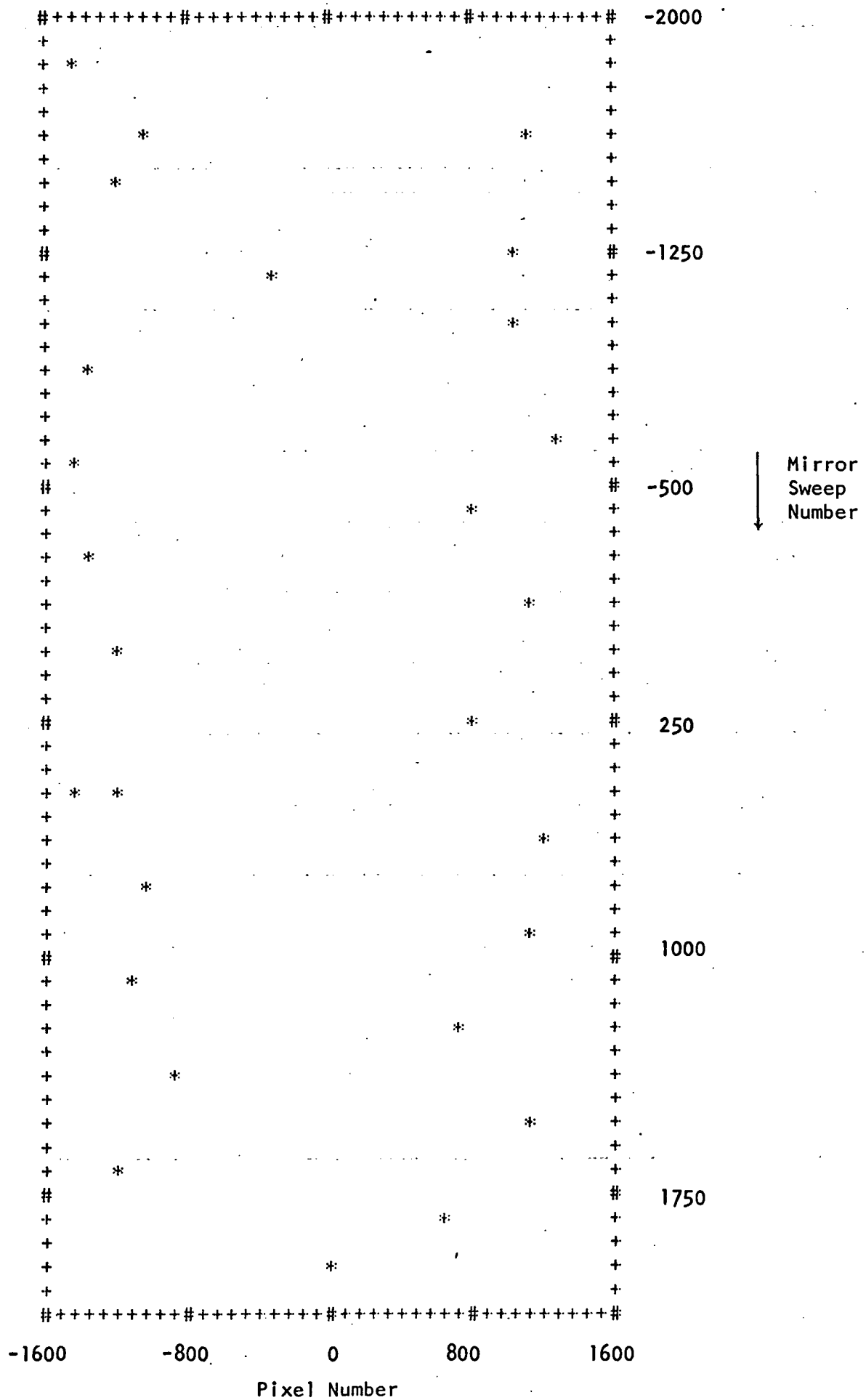

Figure 32 - Control Points Used for Second Pass, 150 Mirror Sweep Spacing, Subset

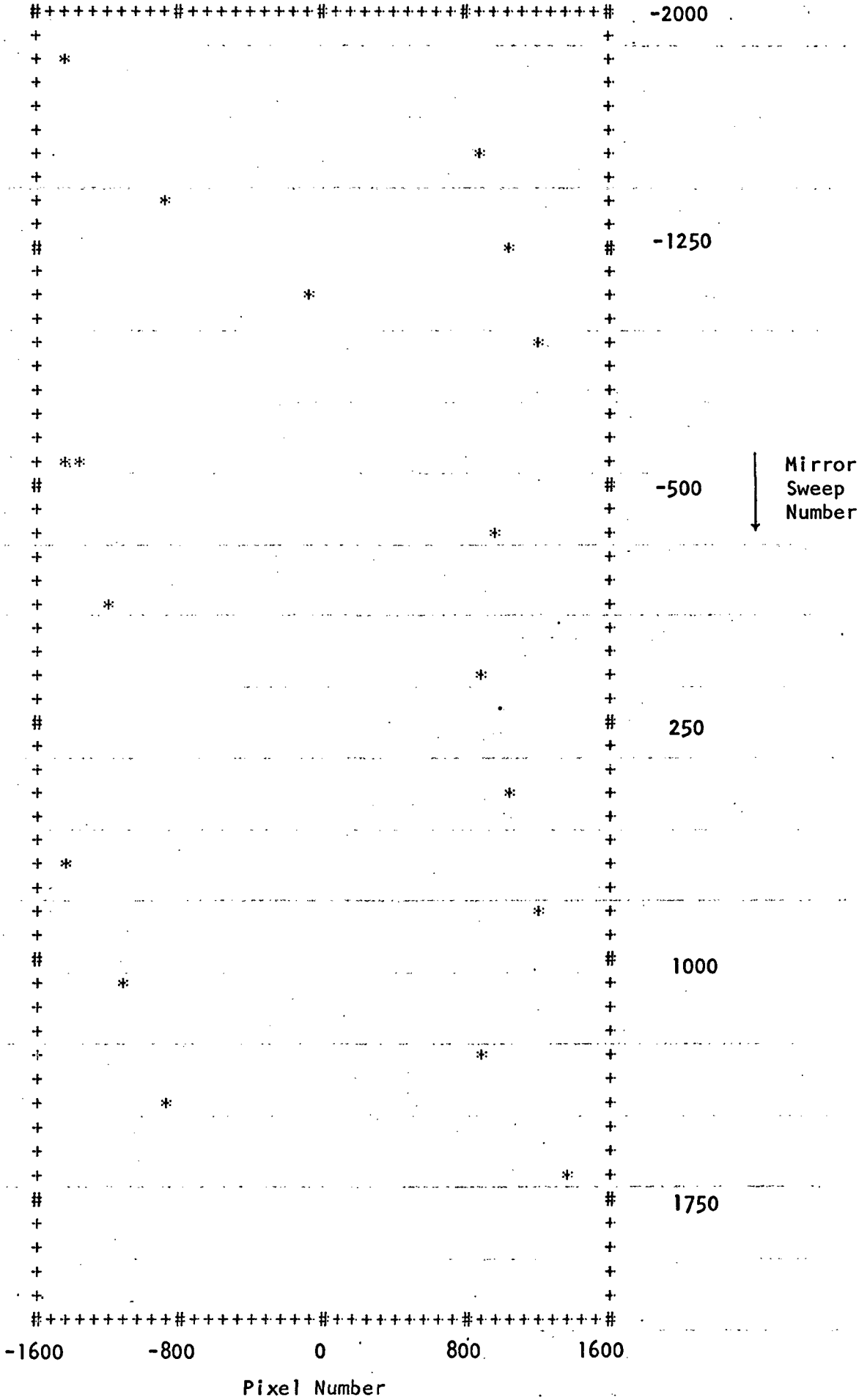

Figure 33 - Control Points Used for Second Pass, 200 Mirror Sweep Spacing, Subset